universität wien

MASTERARBEIT / MASTER'S THESIS

Titel der Masterarbeit / Title of the Master's Thesis

„Atmospheric and surface pathways of the cloud-radiative impact on the circulation response to global warming“

verfasst von / submitted by

Manuel Huber BSc

angestrebter akademischer Grad / in partial fulfilment of the requirements for the degree of

Master of Science (MSc)

Wien, 2022 / Vienna, 2022

Studienkennzahl lt. Studienblatt / degree programme code as it appears on the student record sheet:	UA 066 614
Studienrichtung lt. Studienblatt / degree programme as it appears on the student record sheet:	Masterstudium Meteorologie
Betreut von / Supervisor:	Univ.-Prof. Dr. Aiko Voigt

Abstract

Previous work showed that differences in the near-surface zonal wind response and the poleward midlatitude jet shift under global warming across climate models strongly depend on differences in tropical and midlatitude upper-tropospheric cloud-radiative heating changes. It has emerged that the atmospheric pathway, which is the cloud-radiative impact without having an influence on the sea surface temperature (SST), and the surface pathway, which arises from the cloud-radiative impact on SST, contribute about equally to the poleward circulation expansion in response to global warming in the MPI-ESM model. Building upon the work of Voigt et al. (2019) and Albern et al. (2019), in this study we take a closer look at the surface and atmospheric pathways on a global scale as well as for the North Atlantic, the North Pacific, and the Southern Hemisphere ocean basin. We use the version 2.6.2.2 of ICON, the Icosahedral Nonhydrostatic Modelling Framework, and run it with the climate physics package.

We conduct three simulation sets with the cloud-locking method to determine the contribution of cloud changes to the total circulation response. In the first set of simulations, ICON is coupled to a thermodynamic slab ocean and global warming is mimicked by quadrupling of CO_2. The slab ocean allows for the combined activity of the surface and the atmospheric pathways. In the second set of simulations, climatological SSTs from the first set of simulations are prescribed to isolate the atmospheric pathway, and in the last set of simulations, SSTs are prescribed to the CMIP5 AMIP protocol and global warming is mimicked by a uniform SST increase of 4 K to compare our results to former investigations.

We show that clouds dominate the total circulation response in ICON 2.6.2.2 run with the climate physics package. The atmospheric pathway accounts for half of the total jet shift in the Northern and Southern Hemispheres. Overall, the cloud impact is robustly responsible for a large part of the poleward jet shift across all experimental setups and in all three ocean basins. For the atmospheric as well as the surface pathway, we find a zonally symmetric cloud impact around the jet latitude in all simulation sets and all ocean basins. The surface pathway accounts for approximately two thirds of the poleward shift of the subtropical dry zones in both hemispheres.

We also demonstrate that changes in upper-tropospheric cloud-radiative heating obtained with an upward shift of the present-day cloud-radiative heating are qualitatively able to capture future cloud-radiative heating changes in our simulations. Our findings support the possibility of constraining model biases and intermodel spread using the robust rise of tropical and midlatitude high-level clouds under global warming, as well as observations of current cloud-radiative heating.

Zusammenfassung

Frühere Arbeiten haben gezeigt, dass Unterschiede in der Antwort des bodennahen Zonalwindes und der polwärts gerichteten Verschiebung des Jetstreams, hervorgerufen durch die globale Erwärmung in Klimamodellen, stark von Unterschieden in den Wolkenstrahlungseffekten der oberen Troposphäre der tropischen und mittleren Breitengraden abhängen. Hier unterscheidet man zwischen dem sogenannten „atmospheric pathway", der Wolkenstrahlungseffekte, die keinen Einfluss auf die Meeresoberflächentemperaturen haben, beschreibt und den „surface pathway", welcher Wolkenstrahlungseffekte beschreibt, die Einfluss auf Meeresoberflächentemperaturen haben. Es hat sich herausgestellt, dass beide in etwa zu gleichen Teilen zur polewärtsgerichteten Zirkulationsexpansion durch die globale Erwärmung beitragen. Aufbauend auf der Arbeit von Voigt et al. (2019) und Albern et al. (2019) werfen wir einen genaueren Blick auf den "surface pathway" und "atmospheric pathway" auf einer globalen Skala sowie für den Nordatlantik, Nordpazifik und das Ozeanbecken der Südhemisphäre. Dafür verwenden wir die Version 2.6.2.2 des Atmosphärenmodells ICON und die Parametrisierungen der atmosphärischen Physik, entwickelt für Klimasimulationen.

Wir führen drei Simulationssätze mit der cloud-locking Methode durch um den Beitrag von Wolkenänderungen zur Zirkulationsantwort festzustellen. Im ersten Simulationssatz koppeln wir ICON mit einem thermodynamischen Ozean und die globale Erwärmung wird durch eine Vervierfachung von CO_2 simuliert. Der thermodynamischen Ozean erlaubt die gleichzeitige Aktivität des „surface pathway" und „atmospheric pathway". Im zweiten Simulationssatz schreiben wir die Meeresoberflächentemperaturen durch die Klimatologie der Meeresoberflächentemperaturen des ersten Simulationssatzes vor; so kann der „atmospheric pathway" isoliert werden. Im letzten Simulationssatz schreiben wir die Meeresoberflächentemperaturen durch das CMIP5 AMIP Protokoll vor und die globale Erwärmung wird durch eine einheitliche Erhöhung der Meeresoberflächentemperaturen um 4 Kelvin simuliert. Der letzte Simulationssatz erlaubt uns, unsere Ergebnisse mit vorherigen Untersuchungen zu vergleichen.

Wir zeigen, dass Wolken in ICON 2.6.2.2, betrieben mit der Parametrisierungen, entwick-

elt für Klimasimulationen, die totale Zirkulationsantwort dominieren. Der „atmospheric pathway" trägt zur Hälfte der gesamten polwärtigen Verschiebung des Jetstreams in der Nordhemisphäre und Südhemisphäre bei. Insgesamt ist der Wolkeneinfluss robust für einen Großteil der polwärtigen Jetverschiebung in allen von uns durchgeführten Experimenten sowie über alle großen Ozeanbecken hinweg verantwortlich. Für den „atmospheric" und den „surface pathway" stellen wir einen zonalsymmetrischen Wolkeneinfluss um den Breitengrad des Jetstreams in allen Simulationen und in allen Ozeanbecken fest. Der „surface pathway" trägt zwei Drittel der polwärtigen Verschiebung der subtropischen Trockenzone bei.

Außerdem demonstrieren wir, dass Änderungen des Wolkenheizens in der oberen Troposphäre, approximiert durch die Aufwärtsverschiebung das Wolkenheizens der Gegenwart, qualitative Änderungen des zukünftigen Wolkenheizens abbilden können. Unsere Ergebnisse unterstützen die Möglichkeit zur Einschränkung von Modellfehlern und Modellunterschieden, durch einen robusten Aufstieg von hoher Bewölkung der tropischen sowie mittleren Breitengrade bei globaler Erwärmung, aber auch durch Beobachtungen des Wolkenheizens der Gegenwart.

Contents

1. Introduction

The Earth's climate is changing. Climate classifications for regions worldwide shift (Rubel and Kottek, 2010; Rubel et al., 2017), and with it, the atmospheric circulation. This thesis is about atmospheric circulation changes on a global and regional level and how they are affected by global warming.

Extratropical jet streams, which are either subtropical or midlatitude, are leading metrics for atmospheric circulation. The subtropical jet is primarily driven by the thermally direct Hadley circulation, whereas the midlatitude jet is driven by eddy momentum flux convergence and is thus also known as an eddy-driven or polar front jet (Held and Hou, 1980; Hartmann, 2007). In both hemispheres, most climate models predict a robust expansion of the circulation and a poleward shift of the midlatitude jet streams (Yin, 2005; Barnes and Polvani, 2013; Voigt and Shaw, 2016). But more importantly, as the latitude and strength of the midlatitude jet change, so do the storm tracks, the frequency and duration of synoptic scale blocking patterns, and the heat, momentum, and moisture transport outside of the tropics (Chang et al., 2002; Hoskins and Valdes, 1990; Shaw et al., 2016). Resulting hazards are strong winds and heavy precipitation associated with extratropical cyclones, which lead to wind damage and flooding in coastal and inland regions, but also more severe heatwaves caused by persistent synoptic blocking patterns like in June 2021 on the Pacific Coast of the US and Canada (Philip et al., 2021). This heatwave was estimated to be a 1 in 1000-year event, which would have been at least 150 times rarer without human-induced climate change and also 2°C cooler compared to the time at the beginning of the industrial revolution (Philip et al., 2021). Persistent weather conditions like blocking patterns could be favored by a weakening of the jet and storm tracks in summer (Pfleiderer et al., 2019; Kornhuber and Tamarin-Brodsky, 2021).

1.1 How do Clouds impact the Atmospheric Circulation?

This section provides a theoretical foundation for understanding how changes in atmospheric circulation and midlatitude jet streams are shaped by changes in clouds. It is then followed by the presentation of the concept of the atmospheric and surface pathways in section 1.2.

Section 1.3 explains what uncertainties are connected to the representation of clouds in models. And lastly, section 1.4 is about how models can help us answer fundamental questions about the Earth's climate.

1.1.1 The Cloud-Radiative Effect

Clouds interact with the atmospheric circulation through their cloud-radiative effect. The cloud-radiative effect for shortwave and longwave radiation can be defined as all-sky minus clear-sky radiation for the top of the atmosphere (TOA), the Earth's surface, and within the atmosphere as

$$CRESW_{toa} = S_{toa} - S_{toa}^{clear}, \tag{1.1}$$
$$CRELW_{toa} = OLR - OLR^{clear} \tag{1.2}$$

for **TOA**,

$$CRESW_{sfc} = S_{sfc} - S_{sfc}^{clear}, \tag{1.3}$$
$$CRELW_{sfc} = L_{sfc} - L_{sfc}^{clear} \tag{1.4}$$

for the **surface** and

$$CRESW_{atm} = CRESW_{toa} - CRESW_{sfc}, \tag{1.5}$$
$$CRELW_{atm} = CRELW_{toa} - CRELW_{sfc} \tag{1.6}$$

for **inside the atmosphere** vertically integrated.

All fluxes are defined positive downward and are in units of W m^{-2}. S stands for solar radiation, OLR for the outgoing longwave radiation, hence the emission of thermal radiation into space, and L for the longwave radiation flux at the surface. We will also refer to the atmospheric cloud-radiative effect (ACRE) as cloud-radiative heating throughout this thesis.

12 years of broadband observations showed that in the global annual-mean the shortwave CRE ($\approx$ -47 W m^{-2}) on top of the atmosphere is bigger then the longwave CRE ($\approx$ 26 W m^{-2}) and thus the net effect of clouds on TOA is to cool the Earth system by roughly 20 W m^{-2} (Siebesma et al. 2020, chapter 4.5.2, page 117). One current shortcoming of newer climate models participating in CMIP6, for example, is that through comparisons with satellite observations from *CloudSat/CALIPSO* and *CERES*, it has been found that they overestimate the shortwave CRE and underestimate the longwave CRE which leads to an overall overestimation of the net cooling effect of clouds Miao et al. (2021). *CloudSat/CALIPSO* as well

as *CERES* are part of the A-Train, which is a satellite constellation in a sun-synchronous orbit making daytime observations in the early afternoon. *CloudSat/CALIPSO* combines active lidar and radar measurements, which allows for measurements of small cloud particles, especially ice clouds and larger cloud particles like mid-level clouds near the melting level. *CERES* utilizes passive measurements to quantify the reflected shortwave radiation in the global mean and for the clear sky as well as the emitted longwave radiation at TOA (National Aeronautics and Space Administration, 2022).

Siebesma et al. 2020, chapter 4.6, page 117 further points out that for the top of the atmosphere, the climate impact of clouds can be seen easily because they impact the equilibrium temperature of the Earth directly, but for the surface and within the atmosphere, it is harder. For the surface energy budget, clouds block incoming shortwave radiation but increase incoming longwave radiation. Within the atmosphere, on the one hand, clouds reduce the amount of solar radiation available for absorption by water vapor, and on the other hand, they lengthen the path traveled by radiation by multiple scattering. For computing vertical fluxes at the surface and within the atmosphere, a good understanding of the vertical distribution of clouds is needed.

Fig. 1.1, which is taken from Siebesma et al. 2020, chapter 4.6.1, page 118 shows the estimated CRE on TOA just slightly exceeding the CRE on the surface, leaving as little as ≈ 2 W m^{-2} for within the atmosphere itself and in the global mean. It further shows some key characteristics of the CRE impact on the surface and within the atmosphere on a global scale:

- At high latitudes especially near the poles clouds have a substantial net warming effect on the surface. Because with the decreasing net incoming solar radiation with latitudes, also the cooling effect of reflected solar radiation decreases towards the poles, which leaves the warming effect from the downwelling longwave cloud radiation.
- In areas of the Intertropical Convergence Zone (ITCZ) and in regions of the midlatitude storm tracks clouds have a strong cooling effect on the surface. Because regions of deep moist convection make the atmosphere thick for the spectrum of visible and infrared light which cools the surface, although the longwave warming effect is increased by the moist warm atmosphere with respect to higher altitudes.
- Subtropical marine stratocumulus has less effect on the surface than on TOA. This is visible if one compares the two major stratocumulus regions in the South Pacific westwards of the coast of Peru and in the South Pacific westwards of Angola, as for example defined in Brient et al. (2019). Here, the shortwave cooling effect and the longwave warming effect partly cancel each other out.

- Within the atmosphere the vertically integrated CRE is positive near the equator, neutral in midlatitudes and negative near the poles.

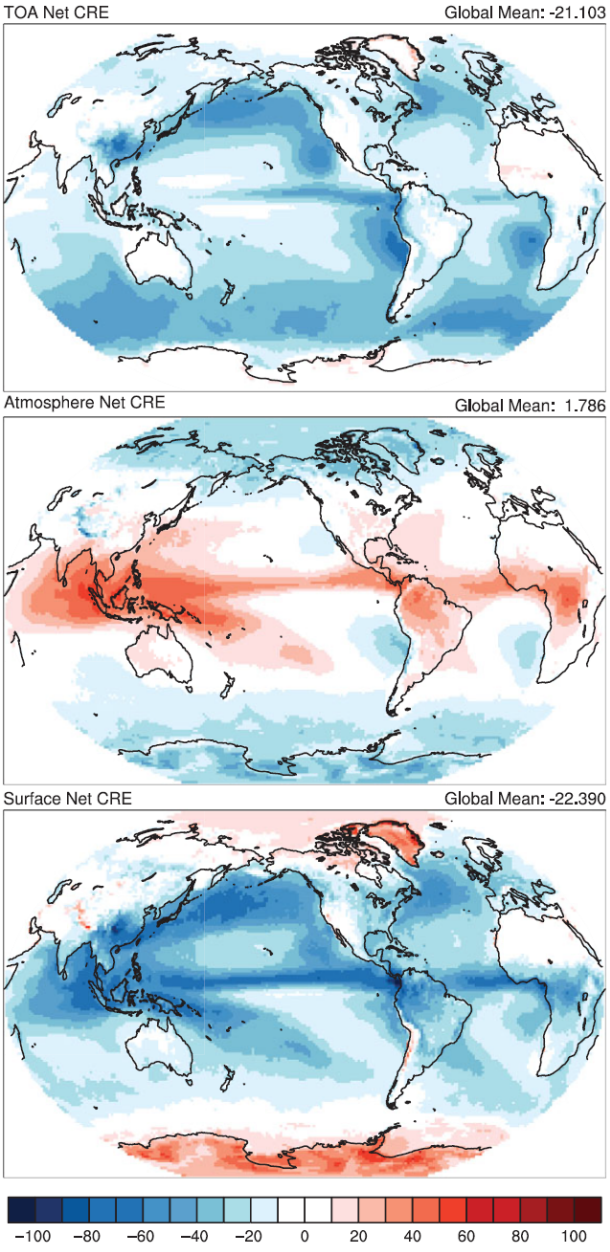

Figure 1.1: Net CRE for TOA within the atmosphere and the surface, taken from Siebesma et al. 2020, chapter 4.6.1, page 118. TOA CRE is determined from broadband observations. For estimations of surface CRE and ACRE, additional observations from space-born lidar and radar, as well as radiative transfer models, are used.

1.1.2 Clouds and Atmospheric Circulation: A Two-Way Coupling

Clouds and atmospheric circulation are tightly coupled. For example, Grise and Medeiros (2016) showed that the circulation changes under global warming, like the poleward jet shift, have a clear imprint on $\mathrm{CRELW_{toa}}$. The same is not so clear for $\mathrm{CRESW_{toa}}$. Grise and Medeiros (2016) discussed that this effect mostly arises from the strong connection between high cloud fraction and $\mathrm{CRELW_{toa}}$, whereas $\mathrm{CRESW_{toa}}$ depends on total cloud fraction. For total cloud fraction, the controlling factors are the vertical velocity in pressure coordinates

at 500 hPa level (ω_{500}) and the estimated inversion strength (EIS). For total cloud fraction, ω_{500} and EIS are competing with each other, where low cloud fraction is shaped mainly by EIS and high level cloud fraction mainly by ω_{500}. We do not want to go too far into this topic, but one can understand this effect on CRE in terms of shifted areas of ascent and descent tied to a poleward shifted midlatitude jet that modifies areas of cloud formation. Thus, the circulation shapes areas where clouds form.

But not just the circulation shapes clouds, clouds also shape the circulation, and for this we need to look at the atmospheric cloud-radiative effect. Clouds warm the atmosphere, predominantly on the cloud bottom via outgoing longwave radiation, or cool the atmosphere, predominantly on the cloud top via absorption of shortwave radiation. Differential heating rates then lead to temperature gradients and thus pressure gradients, which help drive the atmospheric winds. Although for the global atmospheric cloud-radiaitve effect Fig. 1.1 shows just $\approx$ 2 W m^{-2}, regionally, ACRE can reach values as large as 50 W m^{-2}.

ACRE at a certain atmospheric level is the difference between all-sky and clear-sky radiative heating and has units of K day^{-1} (Voigt et al., 2021). The **local heating rate** is defined as

$$\frac{\partial T}{\partial t} = \frac{1}{\rho c_p}\frac{\partial F^{net}}{\partial z} = -\frac{g}{c_p}\frac{\partial F^{net}}{\partial p}. \tag{1.7}$$

F^{net} is the net vertical flux and is defined as positive downward. Thus, a decreasing downward-directed flux (e.g., the shortwave flux) from TOA towards the surface means a heating of the atmosphere. ρ is the density of air and c_p is the isobaric specific heat capacity.

Although the radiative component of cloud heating is an order of a magnitude smaller than the latent heating (Siebesma et al. 2020, chapter 8.4.3, Fig. 8.12) its impact on the atmospheric circulation under global warming is significant and even a dominating factor, which has recently been quantified in models (e.g., Voigt et al. 2019, Albern et al. 2019, Voigt et al. 2021).

Fig. 1.2 from Voigt et al. (2021) shows how the contributions of changes in ACRE and surface CRE under global warming capture the majority of the poleward expansion in the annual-mean zonal-mean wind field pattern, whereas its contribution to the change in the annual-mean zonal-mean temperature field is very small. The poleward circulation expansion can be seen in the dipole of positive (solid) and negative (dashed) change in the zonal-wind field almost throughout the whole depth of the troposphere at around 45°S and 45°N in Fig. 1.2a and 1.2b. What is also visible is the enhanced warming at the poles, especially at the

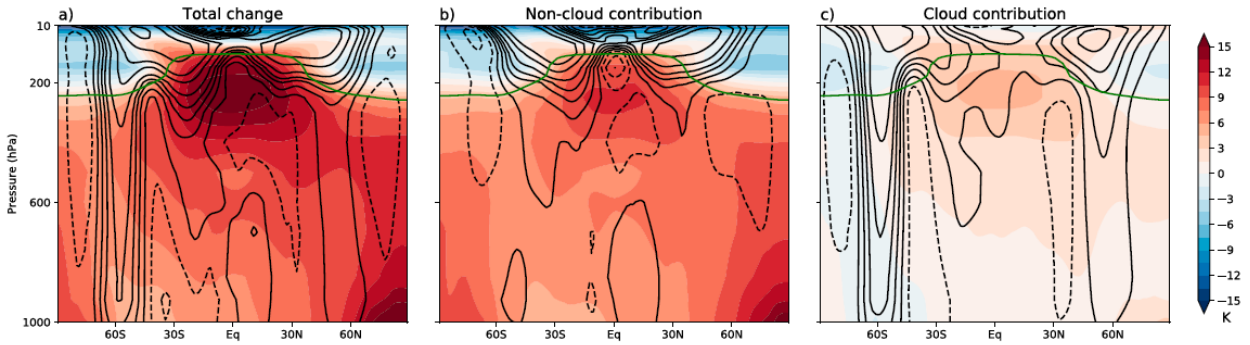

Figure 1.2: Circulation response to quadrupled CO_2 for the MPI-ESM model, taken from Voigt et al. (2019), including the caption: (a) total change in temperature and zonal wind, (b) temperature and zonal wind change attributed to the sum of CO_2 increase and water vapor changes in the absence of cloud changes (noncloud contribution), and (c) temperature and zonal wind change attributed to cloud changes. The temperature change is shown in colors and the wind change by the dashed (negative change) and solid (positive change) black lines, with contour intervals of 1 m s^{-1} between 0 and 3.5 m s^{-1}, 2 m s^{-1} between 5 and 10 m s^{-1}, and 5 m s^{-1} for wind changes with a magnitude larger than 10 m s^{-1}. The green lines in (a)–(c) depict the present-day temperature tropopause.

North Pole in the lower troposphere, called the arctic amplification, and in the upper troposphere above the equator. Two main mechanisms have been identified to play an important role in this outcome:

1. Enhanced surface meridional gradients of absorbed shortwave heating dominated by clouds between the subtropics and high latitudes. Specifically, a cooling of the the surface by clouds around 60°N/S (Ceppi et al., 2014; Voigt et al., 2019). In case of the Southern Hemisphere, a strong relationship between the strength of the enhanced surface gradient and the magnitude of the poleward jet shift in 34 CMIP5 coupled models has been found (Ceppi et al., 2014; Ceppi and Shepherd, 2017).

2. A rise of tropical and midlatitude high-level clouds and with it an enhanced upper tropospheric meridional temperature gradient through changes in longwave heating (Voigt et al., 2019). This anomalous pattern of cloud-radiative heating below the tropopause under global warming amplifies the circulation expansion in terms of poleward shifts of the midlatiude jet, subtropical dry zone, and the Hadley cell edge in realistic model setups with interactive and prescribed SST's (Albern et al., 2020; Voigt et al., 2019; Li et al., 2019). The metrics for the atmospheric circulation expansion are described in section 4.3.

These two mechanisms strengthen the meridional equator-to-pole temperature gradient at lower and upper levels, which increases the baroclinicity throughout the whole troposphere. For this reason, clouds have such a strong impact on the poleward circulation expansion (Voigt et al., 2019; Shaw, 2019). This also means that clouds do not have a strong impact

on the overall magnitude of global warming, but on the spatial pattern of warming, which more strongly depends on the circulation (Grise and Polvani, 2016; Voigt et al., 2019).

To look at the impact of ACRE on the midlatiude circulation closer and quantify the impact of the atmospheric and surface changes in cloud-radiative heating it is useful to apply the concept of the atmospheric and surface pathways, which has been introduced by Voigt et al. (2019).

1.2 The Atmospheric and Surface Pathways

Under global warming clouds either affect or can themselves be affected by surface temperature gradients or atmospheric temperature gradients. Therefore, we divide the cloud-radiative heating into the surface pathway and the atmospheric pathway. Although Voigt et al. (2019) mentions that further simulations with regional cloud changes would be needed to completely account for the roles of lower- and upper-tropospheric ACRE changes like those conducted in Voigt and Shaw (2016), the atmospheric pathway is supposedly dominated by high level clouds. The atmospheric pathway mainly acts through longwave-induced changes in temperature gradients within the atmosphere through the atmospheric component of the cloud-radiative heating. For the atmospheric pathway, it is proposed that ice clouds play a key role.

The surface pathway is likely dominated by low-level clouds, and Voigt et al. (2019) suggested that it mainly acts through shortwave-induced changes in sea surface temperatures affected by the surface component of the cloud-radiative heating. The surface pathway is most active where deep convection is common, e.g. areas of the ITCZ and midlatitude storm track regions. The separation between the atmospheric and the surface pathway can be done via the cloud-locking method and is described in section 4.4.

Voigt et al. (2019) has found that the atmospheric pathway remains relevant even if cloud-radiative interactions with the surface are turned off. Furthermore, regarding the Northern Hemisphere, the atmospheric pathway exceeds the impact of the surface pathway on the poleward jet shift for a global warming experiment with the MPI-ESM under quadrupling of CO_2.

It is worth noting, that the surface pathway, as described in this thesis, includes both cloud-radiative interactions with land and the ocean. If we talk about isolating the atmospheric pathway, interactions of cloud radiation with the ocean surface and sea ice are turned off, while interactions with land masses are still possible. In general, interactions with land

masses compared to interactions with the ocean surface are considered less important for a climatological time span. This is because of the smaller heat capacity of land compared to the ocean.

1.3 Clouds as a Source of Uncertainty in Climate Models

To get a better understanding of the underlying relationships and improve predictions of climate change effects, global climate models (GCMs) are advanced continuously, but large uncertainties remain (Lehner et al., 2020). Zelinka et al. (2020) found that the spread of the global surface temperature response to CO_2 doubling, also known as equilibrium climate sensitivity, in 28 models of the Coupled Model Intercomparison Project 5 (CMIP5) is 2.6 K, around the model mean of 3.3 K. For an explanation of CMIP please see chapter 1.4. This even increases to a spread of 3.8 K around the model mean of 3.9 K in an ensemble of 27 CMIP6 models. It has been concluded that most of this increase arises from physical representations of clouds in the new model generation, which leads to a weaker response of extratropical low-level cloud cover and water content to unforced variations in surface temperature (Zelinka et al., 2020).

With clouds playing such a dominant role in climate sensitivity, recent research has shown that clouds govern the uncertainty of climate change effects in GCMs on global and regional atmospheric circulation (Ceppi and Shepherd, 2017; Voigt and Shaw, 2016; Voigt et al., 2019; Albern et al., 2019). In Albern et al. (2019) cloud-radiative changes contribute one to two thirds of the poleward jet shift in the North Atlantic, North Pacific, and Southern Hemisphere ocean basins, and Voigt et al. (2019) found that the magnitude of direct atmospheric cloud-radiative heating in the upper troposphere and the near-surface zonal wind varies by a factor of 3 in an ensemble of 3 global climate models, with nearly half of the zonal-mean poleward jet shift contributed by cloud-radiative changes just for the atmospheric pathway.

1.3.1 Cloud Parametrization

Although clouds have such a huge impact on the effect of global warming on different scales, their adequate representation in numerical models is a hard task. Because cloud processes range from 1000 km for synoptic scale systems to 1 µm for microphysical processes, the dynamical core of the model cannot explicitly resolve all the processes important for cloud formation. The dynamical core is based on the primitive equations of momentum, mass, energy, and water (Siebesma et al. 2020, chapter 6.2, page 172). Spatial and temporal resolution are limited due to computing power and physical constraints like the Courant–Friedrichs–Lewy condition. Such unresolved processes are called sub-grid processes and include turbulent

transport of heat, moisture, momentum, condensation and evaporation processes, the formation of precipitation, the formation of clouds and cloud cover, and the interaction of clouds with radiation (Siebesma et al. 2020 chapter 6, page 170). The impact of these sub-grid processes on the resolved larger scale needs to be partially or completely parameterized on a statistical and/or physical basis. Typically, these are major sources of systematic errors in weather and climate models. The part of the model that contains the parametrization is referred to as the physics package.

At a minimum, the parametrization scheme of clouds needs to provide 3 microphysical variables: the horizontal cloud fraction of every gridbox, the associated cloud liquid water and cloud ice, and the vertical overlap of the cloud fraction in a vertical column (Siebesma et al. 2020, chapter 6.6.1, page 198). Siebesma et al. (2020) describe further that these three properties are important because they are then used in the radiation scheme.

There are some uncertainties associated with this. For example, the sub-grid variability of total water and temperature. This is taken into account by probability density functions, which can be of different shapes depending on the distribution of the total cloud water in the grid boxes (Tompkins, 2005). Another uncertainty is the cloud overlap in the vertical, which is important for total cloud cover and impacts, for example, the shortwave cloud-radiative effect at the top of the atmosphere (TOA). Also, cloud inhomogeneity itself needs to be taken care of because the mean albedo of an inhomogeneous cloud is smaller than the albedo of the average cloud liquid water content in the grid box of interest, which means that the cloud-radiative effects (CRE) depend in a nonlinear manner on cloud condensate (Fu and Liou, 1993). In some models, this is approximated by a correction factor, which reduces the cloud optical depth used in the radiation scheme. Newer models use the Monte Carlo independent column approximation, which calculates the radiative transfer for a few randomly chosen wavelengths for each sub-box. The assumption there is that the error made in not using all wavelengths will cancel out itself if done for a large enough number of sub-boxes. Fig. 1.3 produced by Mauritsen et al. (2012) shows different applications for model tuning in the ECHAM model as an example of the sources of uncertainty associated with cloud parametrizations.

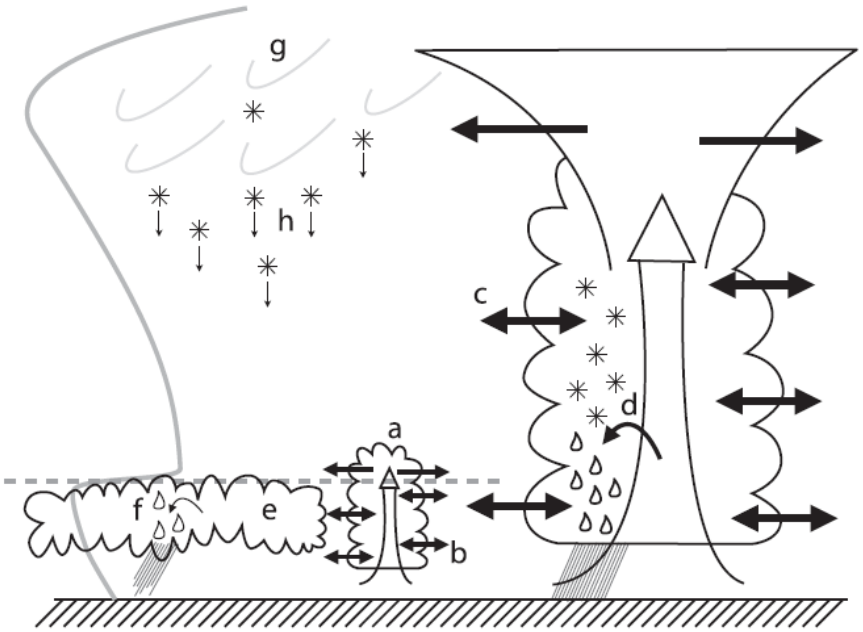

Figure 1.3: Example of tuning applications taken from Mauritsen et al. (2012), including the caption. Illustration of the major uncertain climate-related cloud processes frequently used to tune the climate of the ECHAM model. Stratiform liquid and ice clouds, and shallow and deep convective clouds are represented. The grey curve to the left represents tropospheric temperatures and the dashed line is the top of the boundary layer. Parameters are a) convective cloud mass-flux above the level of non-buoyancy, b) shallow convective cloud lateral entrainment rate, c) deep convective cloud lateral entrainment rate, d) convective cloud water conversion rate to rain, e) liquid cloud homogeneity, f) liquid cloud water conversion rate to rain, g) ice cloud homogeneity, and h) ice particle fall velocity.

1.4 How can Model Simulations help?

Even if GCMs are not perfect representations of the Earth system, we need them to be able to determine cause-and-effect relationships that are difficult to capture in observations. They also help to fill in gaps in observational data, which may be limited to specific time periods, locations, and/or variables. But furthermore, through model simulations, we are able to draw conclusions from experiments like increasing the temperature of the ocean surface, experiments that would be impossible to carry out in real life. If multiple simulations are performed with different climate and weather models under a comparable framework and the outcomes of these simulations coincide with each other, chances are some basic physical mechanisms can be determined.

Focusing on future projections, GCMs provide a toolbox in which climate impacts from increased greenhouse gases like CO_2 can be studied. More specifically and regarding this thesis, if mechanisms by which cloud-radiative heating impact the circulation in models are

understood better, a more targeted observational analysis may be possible. This could help to constrain correct and incorrect model behaviors in simulating the cloud impact on the circulation (Voigt et al., 2021). Intermodel spread concerning the midlatitude jet response could be reduced, and hence the projections of regional global warming impacts could be improved.

Because GCMs are developed by scientific communities around the world, a standardized framework for comparing results and model-reliability has been developed called AMIP (Atmospheric Model Intercomparison Project) and CMIP (Coupled Model Intercomparison Project). AMIP is a standard experimental protocol for global atmospheric general circulation models (AGCMs). It originally provided observed monthly means of sea surface temperature and sea ice as boundary conditions for the years 1979-1988, and a set of output variables which every participating AGCM needed to meet. It serves the purpose of a systematic comparison and validation of the performance of atmospheric GCMs on seasonal and interannual time scales (Gates, 1992). It is not used for climate change projections.

CMIP also serves the purpose of providing a standardized simulation framework, but on the other hand, it is specifically designed to better understand past, present, and future climate changes. Here, the AGCM is coupled to an ocean model, which also includes interactive sea ice. Its set of experiments assess historical climate periods, investigate the causes of the spread in future projections, and, with idealized experiments, try to better understand model responses. Aquaplanet simulations, for example, fall in the latter category. In this thesis, however, a SSTCLIM-setup under the CMIP5 label is used. It aims to evaluate certain model behaviors, especially fast responses, under a more realistic view and falls into the second category (Taylor et al., 2012). With “fast responses”, we mean climate system responses that occur from changes in CO_2, where no changes in SSTs have yet been possible. The SSTCLIM-setup is further described in section 4.2.

2. Motivation and State of Research

Clouds, circulation, and climate sensitivity were one of the seven major challenges defined by the World Climate Research Programme (WCRP) for the last decade. But still, climate models do not agree on the magnitude of the cloud-radiative impact on atmospheric circulation changes (Voigt et al., 2019).

The most recent modeling framework, CMIP6, is specifically designed to answer three broad questions (Eyring et al., 2016):

1. How does the Earth system respond to forcing?
2. What are the origins and consequences of systematic model biases?
3. How can we assess future climate changes given internal climate variability, predictability, and uncertainties in scenarios?

Because cloud-radiative effects play a role in all three of these questions, they have already been the subject of a considerable amount of research in the CMIP5 era (Taylor et al., 2012) but also in CMIP6 (Eyring et al., 2016), especially in terms of climate sensitivity. As we focus on the atmospheric cloud-radiative effect, we are specifically interested in the cloud-circulation coupling, where large uncertainties remain.

Models robustly predict a poleward jet shift in the annual-mean zonal-mean, but the intermodel spread in these projected shifts differs by several degrees (Voigt and Shaw, 2016). Voigt and Shaw (2016) evaluated an ensemble of CMIP5 models for different setups, including idealized aquaplanet studies, studies with coupled atmospheric-ocean models (interactive SSTs), as well as atmospheric-only simulations (prescribed SSTs), including realistic land boundary conditions. In this thesis, we aim to extend the range of the coupled and atmosphere-only experiments with the newly released ICON version.

Voigt and Shaw (2016) concluded that the rise of high-level clouds, warming the upper troposphere, as well as the rise and poleward shift of midlatitude high-level clouds, warming the midlatitude upper troposphere, leads to a robust poleward jet shift and an expansion

of the Hadley circulation. Also, a cloud change initiated cooling of the high latitude lower troposphere has the potential to shift the midlatitude jet polewards, but with a smaller impact than the tropical and midlatitude cloud changes. Although the latter effect is not robust across models, these two findings point out the importance of ACRE on atmospheric circulation change.

A similar outcome has been found in other studies (e.g. Ceppi et al. 2014, Ceppi and Shepherd 2017, Voigt et al. 2019, Albern et al. 2020). Also, Li et al. (2019) found that the atmospheric CRE of rising high clouds is most likely a new robust thermodynamic constraint on climate change. Hence, an improvement in the understanding of the cloud-circulation coupling in climate models may help to restrict model biases and intermodel spread. This could lead to a more precise quantification of how cloud-radiative heating influences the jet shift, and more accurate projections of the global and regional effects of climate change may be possible.

Voigt et al. (2019) showed that the radiative impact of clouds on the circulation can be quantified with the cloud-locking method. Using it in a specific way, one can separate the cloud-radiative effect into the atmospheric pathway and the surface pathway. As discussed in chapter 1.2, the atmospheric pathway arises from changes in atmospheric cloud-radiative heating and tends to be dominated by high-level clouds, while the surface pathway arises from changes in surface cloud-radiative heating which tends to be dominated by low-level clouds.

It has been found that the magnitude of the atmospheric pathway strongly differs from one model to another. These model differences have been linked to model differences in the present-day cloud radiative heating, which are large in the tropical upper troposphere. Additionally, all models analyzed in Voigt et al. (2019) show large discrepancies in simulating the cloud-radiative heating in the present-day climate compared with observations from *CloudSat/CALIPSO*.

Given this uncertainty, in this thesis we study the atmospheric and surface pathways of the cloud-radiative impact on the circulation response to global warming with the version 2.6.2.2 of the atmospheric component of ICON using the climate physics package. We either prescribe the SST or couple the atmospheric component to a slab ocean, which enables the separation of the cloud impact into the atmospheric and surface pathways following Voigt et al. (2019).

3. Research Questions and Outline

In order to structure the thesis and evaluate its outcome we formulate the following research questions. Question 1 is answered in section 5.1, the results of Question 2 are discussed in section 5.2 and the results of Question 3 are presented in section 5.3.

Question 1

What is the role of clouds in setting the zonal-mean circulation response to warming on a global scale and how is the cloud impact distributed between the atmospheric and surface pathways?

Because this separation of the cloud-radiative impact into the atmospheric and surface pathways with a GCM coupled to a slab ocean has been done only once with the MPI-ESM it is interesting and potentially revealing to study the separation in an additional model. One goal is to evaluate if the dominance of the atmospheric pathway, which accounts for half of the cloud contribution to the poleward circulation expansion in the Southern Hemisphere (SH) and for even more in the Northern Hemisphere (NH) in Voigt et al. (2019), is robust, meaning it can be reproduced. For this, we will quantify the global warming impact on the shift in the midlatitude jet stream and the subtropical latitude of net precipitation, divided into the atmospheric and surface pathways. Both circulation metrics are further description in section 4.3.

Question 2

Focusing on the three ocean basins of the North Atlantic, North Pacific, and Southern Hemisphere, what is the relative role of the atmospheric and surface pathways in the jet response regionally?

Because the cloud-radiative impact on the jet response is not just relevant in the zonal mean, but even more so on a regional scale, shaping climate change effects regionally, we will add to the work of Albern et al. (2019). How the jet shift varies locally, specifically in the three ocean basins, has been studied less. Therefore it is important to expand the range of available simulation results in order to assess the intermodel spread. Albern et al. (2019) found a poleward jet shift in the North Atlantic, the North Pacific, and the Southern Hemisphere. For the North Atlantic half and for the North Pacific two thirds of this shift have been attributed to the cloud-radiative impact, whereas in the Southern Ocean basin this contribution is about one third. Albern et al. (2019) also depicts a significant jet strength increases in the North Atlantic and the Southern Hemisphere, where one third of this strengthening in the Southern Hemisphere arises from the cloud-radiative impact and half in the North Atlantic. In the North Pacific, just a very weak strengthening of around 0.5 m s^{-1} was found. These results from Albern et al. (2019) are for the atmospheric pathway only. Hence, we will expand the available simulation results for the three main ocean basins by enabling the activity of the surface pathway with a slab ocean.

Question 3

What are the changes in cloud-radiative heating in ICON-ESM under global warming, and are these changes captured by an upward shift of the present-day cloud-radiative heating?

In previous work, a broad arc of anomalous cloud-radiative heating in the tropics and midlatitudes below the tropopause under global warming was found, being a prominent feature in the aquaplanet work of Voigt and Shaw (2016) and in an ensemble of three GCMs with realistic land boundary conditions in Voigt et al. (2019). This arises from an upward shift of tropical and midlatitude high-level clouds. The qualitative shape of the heating pattern in the tropical and midlatitude upper troposphere found in Voigt et al. (2019) seems to be robust across models but varies greatly in magnitude. This difference translates into differences in the atmospheric cloud-radiative impact on the circulation change. Higher magnitudes of anomalous heating equal a stronger response in atmospheric circulation.

In Voigt et al. (2019) it has been suggested that the difference in the changes of present-day upper-tropospheric cloud-radiative heating contributes much to the difference in changes of upper-tropospheric cloud-radiative heating under global warming. The applied upward-shift

framework showed good agreement between the changes in present-day and future changes in cloud-radiative heating under global warming for the midlatiudes. For the tropics, two out of three models (MPI-ESM, IPSL-CM5A) agreed qualitatively, although the magnitude in the difference between the upward shifted present-day and future cloud-radiative heating was much higher than for the midlatitudes. One model (ICON with the NWP-physics package) showed large discrepancies. This discrepancy in ICON-NWP, which is the same model as used in Albern et al. (2019), has been linked to a large increase in cloud ice in the tropics under global warming. A similar increase was not found in the other two models. Even more surprising, the present-day cloud-radiative heating of no model agreed well with observations from *CloudSat/CALIPSO*, not even the ERA-Interim reanalysis.

Given that changes in upper-tropospheric cloud-radiative heating are important for the magnitude of changes in atmospheric circulation, we will compare the vertical distribution of cloud fraction and ice with the results of Voigt et al. (2019), repeat the application of the upward shift framework, and evaluate its potential for ICON version 2.6.2.2 with the climate physics package.

4. Methodology

This chapter gives an overview of the methods used to answer the research questions. Section 4.1 starts with a description of the ICON model. Section 4.2 shows the simulation setup and the three different simulation sets we performed for this thesis. Section 4.3 presents the metrics we use to assess changes in atmospheric circulation under global warming. Section 4.4 describes the cloud-locking method, which allows the decomposition of the total circulation response into the response which arises from changes in clouds, water vapor, or SST/CO_2. Section 4.5 presents the vertical shift framework used to answer Question 3, and section 4.6 explains the partial-radiative perturbation calculations, which is a method to diagnose cloud-radiative heating changes in model simulations under global warming.

4.1 The ICON Model

The development of the Icosahedral Non-hydrostatic model (ICON) framework is done by the German Weather Service (DWD) and the Max Planck Institute for Meteorology, as well as many partner institutions, like the Institute of Meteorology and Climate Research at the KIT or the German Climate Computing Center (DKRZ) (Lang, 2021). It can be used for climate simulations as an Earth system model (ESM), for numerical weather predictions (NWP) and for large eddy simulations (LES) with high resolution. ICON-ESM means that the atmospheric component (ICON-A), the model for land (JSBACH), and the ocean model (ICON-O) are coupled (Max-Planck-Gesellschaft (MPG) zur Förderung der Wissenschaften e.V., 2017). This enables the exchange of water, energy, and momentum between all those components and allows for the representation of the important effect of the ocean on the climate system in model simulations. The coupling of the different components of the ICON-ESM is achieved by the coupling software YAC for Earth system models developed by DKRZ. For this thesis, we use the atmospheric component of ICON-ESM coupled with JSBACH and a 50 m deep slab ocean. Because of computational restrictions, we just simulate the upper 50 m of the total ocean depth. The slab ocean setup is described in subsection 4.2.2.

4.2 Simulation Setup

For our simulations, we use a realistic setup that includes continents, sea ice, and a seasonal cycle like in Voigt et al. (2019), with ICON version 2.6.2.2 and the climate-physics package that originates from ECHAM6. In the following, we will refer to this setup as "ICON-ESM". The horizontal resolution is R2B04, which corresponds to approximately 160 km, and a vertical resolution of 47 model levels up to 75 km. The model time step is 20 minutes. Greenhouse gases are kept constant at values averaged over the 1979-2008 AMIP period (CO_2 = 359 ppmv, CH_4 = 1693 ppbv, N_2O = 311 ppbv, CFC_{11} = 237 pptv, CFC_{12} = 462 pptv). Ozone is set to a monthly climatology of the years 1979-2008 and aerosol long- and shortwave optical properties are prescribed to monthly values of the year 2000 of the Max-Planck-Institute aerosol climatology version 1 as introduced in Kinne et al. (2013). Total solar irradiance is set to the 1979–1988 time series average value of 1361.371 W m^{-2} provided for CMIP5. These settings are in line with Voigt et al. (2019). For our analysis, we performed the following 3 simulation sets.

4.2.1 SSTCLIM

This simulation set refers to an AMIP-like setup. For this simulation set, we call the present-day simulation **"SSTCLIM-CTL"**. For SSTCLIM-CTL we prescribe SST and sea-ice cover to the climatological monthly-mean values of the AMIP period 1979-2008 (Taylor et al., 2012). The global warming effect is simulated with a uniform 4-K SST increase because Albern et al. (2019) found that the cloud-radiaive impact on the jet stream do not strongly depend on the pattern of the SST increase. For this simulation set, we call the warming simulation **"SSTCLIM-WRM"**. Because sea ice is still prescribed to the present-day simulation and greenhouse gases are kept constant, the SST effect is isolated. In total, 30 years are simulated, with the first year removed to avoid spinup effects. The surface temperature of the control simulation has a spatial and climatological mean of 288.1 K and the warming simulation of 292.6 K, which adds up to a total warming of 4.5 K. Fig. 4.1 shows the prescribed SST and sea-ice cover used in the SSTCLIM-CTL simulation.

4.2.2 SLAB

SLAB refers to the simulation set with a thermodynamic slab ocean. Here, the atmospheric model is coupled to a 50 m deep thermodynamic slab ocean, which enables a cloud impact on SSTs and sea ice and, therefore, the simultaneous activity of the atmospheric and surface pathways. The simulated 50 m represents the upper layer of the ocean, which is well mixed and allows for the ocean energy transport, also called q flux. The q flux is diagnosed from a simulation with the same present-day experimental setup as in SSTCLIM-CTL, and means

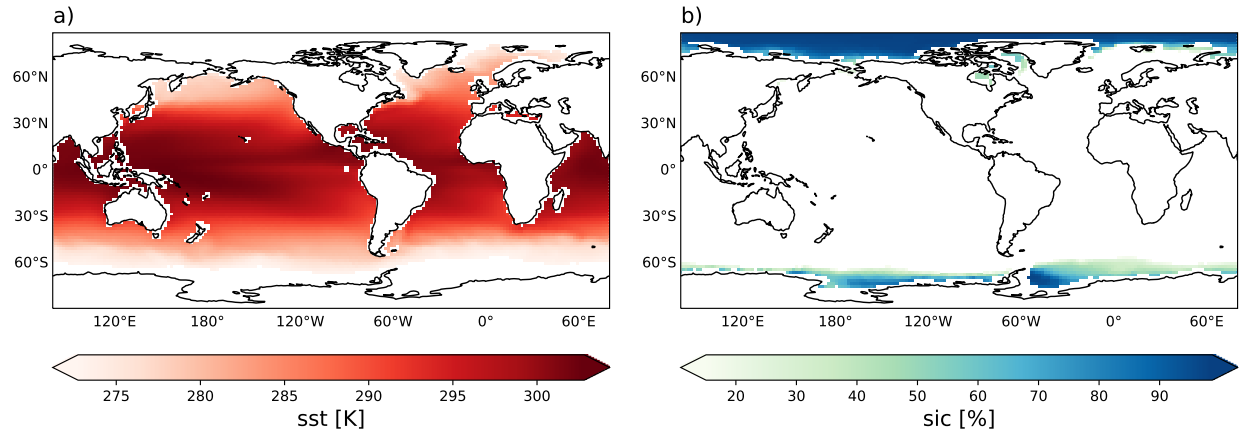

Figure 4.1: (a) Annual-mean SST and (b) annual-mean sea-ice cover from CMIP6 for which SSTCLIM-CTL is prescribed to. For (a) regions with sea-ice cover greater than 15% are masked. For (b), regions with sea-ice cover less than 15% are masked. Land, lakes, and glaciers are masked with ICON's native mask for version 2.6.2.2.

that SST and sea-ice cover are interactive and respond to changes in CO_2 and clouds. Here, in total, 40 years are simulated with 10 years removed to avoid spinup effects. We checked that after 10 years, outgoing longwave and shortwave radiation, as well as surface temperature and sea-ice cover, are in a state of equilibrium. For the mimicking of the global warming effect, the CO_2 value is quadrupled. This simulation is referred to as **"SLAB-WRM"**. We call the simulation without increased CO_2 **"SLAB-CTL"**.

The surface temperature has a spatial and temporal mean of 288 K in the control simulation and 294.7 K in the global warming simulation. This means a total warming of 6.7 K, which is around 2 K higher than in SSTCLIM. Fig. 4.2 shows the difference in the annual-mean SST and sea-ice cover for SLAB-WRM and SLAB-CTL. It can be seen that the strongest reduction in sea ice occurs where the warming of the SSTs is strongest, i.e., at the Antarctic coast in the South Atlantic.

4.2.3 SSTSLAB

With the SSTSLAB simulation setup, we isolate the atmospheric pathway of the slab ocean simulation. SST and sea-ice cover are prescribed to either the climatology of the SLAB-CTL or the SLAB-WRM simulation. This way, SST and sea-ice cover are once again not interactive anymore and therefore can not change due to cloud changes. We apply the same nomenclature as in the simulation sets before, thus the control simulation of this simulation set is called **"SSTSLAB-CTL"** and the warming simulation **"SSTSLAB-WRM"**. The surface temperature of the control simulation has a spatial and temporal mean of 287.9 K and the warming simulation of 294.6 K, being very close to the values of SLAB.

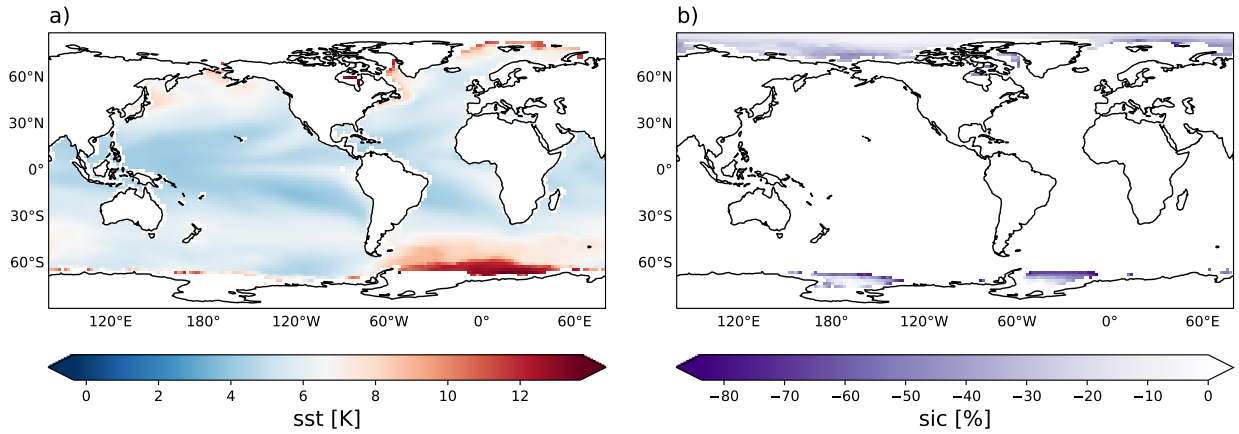

Figure 4.2: (a) Change of annual-mean SST and (b) annual-mean sea-ice cover for SLAB setup under quadrupling of CO_2. In the color scale of (a) the color white corresponds to the spatial and temporal-mean warming of 6.7 K. For (a) regions with sea-ice cover greater than 15% are masked. For (b), regions with sea-ice cover less than 15% are masked. Land, lakes, and glaciers are masked with ICON's native mask for version 2.6.2.2.

4.3 Circulation Metrics

4.3.1 The Midlatitude Jet Stream

There are two major jet streams: the subtropical jet, which is mainly driven by the angular momentum transport of the thermally direct Hadley circulation, and the polar front jet, which results from the eddy momentum flux convergence by atmospheric waves that develop in regions of enhanced baroclinicity (Held and Hou, 1980). Hence, the latter is also called eddy-driven jet or midlatitude jet stream. The midlatiutde jet is well known to have a strong influence on heat, moisture, and momentum transport outside of the tropics (Chang et al., 2002; Hoskins and Valdes, 1990; Shaw et al., 2016) and is thus an important metric in characterizing the effects of regional climate change. Therefore, in this thesis, we focus on the midlatitude jet stream.

For the Northern Hemisphere, like in Voigt et al. (2019) and Albern et al. (2019) we do a zonal mean of the jet latitude at the 850 hPa level (u_{850}), then search for the latitude of the maximum velocity between 25°N and 70°N (25°S and 70°S respectively for the Southern Hemisphere) and interpolate on a 0.01° latitude grid between the two neighboring grid points. On the interpolated grid, we apply a quadratic fit. The maximum of the quadratic fit gives the jet strength u_{jet} and its latitude position ϕ_{jet}. We look at the 850 hPa level because at this level, due to its quasi-barotropic character, the midlatitude jet is still visible where the subtropical jet is not. Subtropical and eddy-driven jets are frequently merged in the upper troposphere, making differentiation difficult at higher levels.

For the North Atlantic we search for the maximum velocity and apply the quadratic fit between 60°W and 0° and for the North Pacific we search for the maximum velocity between 135°E and 125°W.

4.3.2 Subtropical Dry Zones

The second metric for the atmospheric circulation we look at is the zone of zero net precipitation. For this we subtract evaporation (E) from precipitation (P) and search for the latitude where the result is 0 (P-E=0). We also interpolate around the latitude where P-E=0 and its two neighboring grid points at a 0.01° grid to get a more precise result.

Other than in Voigt et al. (2019) we do not use the Hadley cell edges for the analysis because, with the climate physics package, the ICON does not show a well defined transition from the Hadley cell to the Ferell cell anymore.

4.4 Cloud-Locking Method

We build on the work of Voigt et al. (2019) and Albern et al. (2019). The cloud-locking method allows for the quantification of the surface and the atmospheric pathways. This is achieved by breaking the radiative interactions between clouds, water vapor, SST, and the atmospheric circulation by prescribing the radiative properties of clouds and water vapor to the model's radiative transfer scheme. Using this method, it is possible to isolate the impact of clouds on circulation change under global warming from the effects of increased water vapor and SST/CO_2.

In total, we perform 10 simulations for each simulation set. A control simulation, which represents the present-day climate for each set and a simulation which mimics global warming, as discussed in chapter 4.2. In both of this simulations no properties are locked. Then we perform eight additional simulations in which we prescribe SST/CO_2 (F) and lock the radiative properties of clouds (C) and water vapor (W): F1C1W1, F1C1W2, F1C2W1, F1C2W2, F2C1W1, F2C1W2, F2C2W1, F2C2W2. The index 1 represents the values from the control simulation and index 2 the values from the global warming simulation.

The calculation of the total response to warming and its decomposition into the cloud-radiative, water vapor, and SST/CO_2 using the cloud-locking method is presented below.

4.4.1 Total Locked Response

We define the total locked response on any given variable as

$$\Delta X_{lock} = X_{F2C2W2} - X_{F1C1W1}. \tag{4.1}$$

4.4.2 Total Free Response

The total free response on any given variable of the combined effects of the SST/CO_2 increase, the cloud-radiative changes, and the water vapor changes is given by

$$\Delta X_{free} = X_{CTL} - X_{WRM} = X_{F2C2W2} - X_{F1C1W1} + Res. \tag{4.2}$$

The residual occurs due to the application of the cloud-locking method and is discussed below.

4.4.3 Impact of Changes in SST/CO_2, Cloud Radiation and Water Vapor

The contribution of the **cloud-radiative changes** is given by

$$\Delta X_{cloud} = \frac{1}{4}\Big[(X_{F1C2W1} - X_{F1C1W1}) + (X_{F1C2W2} - X_{F1C1W2}) + (X_{F2C2W1} - X_{F2C1W1}) + (X_{F2C2W2} - X_{F2C1W2})\Big], \tag{4.3}$$

and the contribution of the **water vapor changes** is given by

$$\Delta X_{vapor} = \frac{1}{4}\Big[(X_{F1C1W2} - X_{F1C1W1}) + (X_{F1C2W2} - X_{F1C2W1}) + (X_{F2C1W2} - X_{F2C1W1}) + (X_{F2C2W2} - X_{F2C2W1})\Big]. \tag{4.4}$$

The contribution of the **SST/CO_2 increase** in absence of radiative changes in clouds and water vapor therefore is

$$\Delta X_{SST/CO_2} = \frac{1}{2}\Big[(X_{F2C1W1} - X_{F1C1W1}) + (X_{F2C2W2} - X_{F1C2W2})\Big]. \tag{4.5}$$

The cloud-radiative, water vapor, and SST/CO_2 impact sum up to $X_{F2C2W2} - X_{F1C1W1}$, so that

$$\Delta X = \Delta X_{cloud} + \Delta X_{vapor} + \Delta X_{SST/CO_2} + Res. \tag{4.6}$$

Hence, the **residual** is given by

$$\begin{aligned} Res = \Delta X_{free} - \Delta X_{lock} &= (X_{WRM} - X_{CTL}) - (X_{T2C2W2} - X_{T1C1W1}) \\ &= (X_{WRM} - X_{CTL}) - (\Delta X_{SST/CO_2} + \Delta X_{cloud} + \Delta X_{vapor}). \end{aligned} \quad (4.7)$$

The residual can arise from the internal variability of the different simulations in one simulation set because of the chaotic nature of the Earth system. But the residual can also arise due to the decorrelation of the radiative properties of clouds and water vapor from the instantaneous circulation by the cloud-locking method. Because the prescribed radiative properties do affect just the radiation scheme of the model, it can for example happen, that the cold-sector radiative properties of an extratropical cyclone are prescribed in the warm-sector and vice versa (Voigt et al., 2019). In chapter 5, we will study the residual and show that it is small for most circulation changes. A small residual is a prerequisite for the cloud-locking method, otherwise the method is difficult to interpret.

4.5 Vertical Shift Framework and the Fixed Anvil Temperature Hypothesis (FAT)

The upward shift framework as we use it here and as it was also used in Voigt et al. (2019) was first derived from the moist primitive equations in Singh and O'Gorman (2012). It can be applied to approximate the response of many variables to warming, like the changes in zonal- and time-mean atmospheric temperature, the lapse rate, the relative humidity, or the meridional mass streamfunction. We look at the changes in upper-tropospheric cloud-radiative heating for the tropics and the midlatitudes. The parameter β determines the magnitude of the shift, where β is defined as

$$\frac{\beta - 1}{\delta T_{BL}} \approx 0.04 K^{-1}. \quad (4.8)$$

δT_{BL} is the difference in temperature at a fixed pressure level near the top of the boundary layer and the constant 0.04 K^{-1} is dependent on the lapse rate. To calculate δT_{BL}, we follow Voigt et al. (2019) and use the 850 hPa level.

The upward shift framework works because of the robust rise of the high level convective clouds in the tropics and the midlatitudes under global warming, where the fixed anvil temperature (FAT) hypothesis of Hartmann and Larson (2002) can be applied. The FAT hypothesis states that convective anvil clouds remain approximately at the same temperature as the climate changes. Because of convection near the equator, somewhere at around 200 hPa, the radiative cooling of water vapor is not sufficient enough anymore to maintain

the radiatively driven convective layer. This happens because the decrease in water vapor pressure as the temperature decreases means a reduction of water vapor molecules. This mechanism defines the level where the maximum of clear sky mass convergence and detrainment occurs, which in turn generates the cloud anvil. Farther polewards, at the descending branch of the Hadley cell, the large scale subsidence is not balanced by clear sky radiative cooling anymore and hence leads to downward motion. Because the relationship between the phase transition from water vapor to water droplets is defined by the Clausius–Clapeyron equation and the temperature where this transition happens is constant throughout all climates, the cloud-anvil temperature is fixed, even if the depth of the troposphere increases or the surface warms. This implies a positive longwave cloud feedback at the tropical latitudes because the difference between the cloud top temperature and the surface temperature increases (Siebesma et al. 2020, chapter 13.4.3.1, page 375). A similar mechanism holds for the extratropical storm track regions (Thompson et al., 2017).

One limitation of the upward shift framework is that the solution of the transformation is only valid above the well mixed boundary layer because the derivation assumes an inviscid atmosphere. Another limitation is that β is dependent on the lapse rate. Singh and O'Gorman (2012) found that the error of the transformation in the case of a pseudo-adiabatic parcel ascent increases with the surface temperature. However, since our analysis is on a global scale, with average surface temperatures well below 300 K, this should not matter.

4.6 Partial-Radiative Perturbation Calculations (PRP)

The partial-radiative perturbation calculations are implemented in the same way as in Voigt and Shaw (2016) and Voigt et al. (2019) and were first introduced by Wetherald and Manabe (1988). It is a two-sided diagnostic where the impact of the radiative changes from clouds and/or water vapor can be calculated separately offline, with one or both prescribed to the CTL or WRM simulation, without changes in the atmospheric temperature. This is not possible when cloud-radiative heating changes are obtained from the all-sky minus clear-sky fluxes like described in subsection 1.1.2.

The impact of changes in clouds between two climate states is given by

$$\left.\frac{\partial T(\phi,p)}{\partial t}\right|_{PRP} = R(T_{CTL}, q_{CTL}, c_{WRM}) - R(T_{CTL}, q_{CTL}, c_{CTL}). \tag{4.9}$$

R is the temperature tendency, which is calculated by the radiative transfer scheme of the model. The parameter T is the atmospheric temperature at pressure p and latitude ϕ. q stands for the specific humidity and c for the radiative properties of clouds. The subscript

CTL means that the variables are used from the present-day-like control simulation, whereas WRM means they are used from the global warming simulation. Because Eq. 4.10 provides the impact of the radiative properties from clouds in the global warming simulation on the present-day climate, to get a more precise result, we also calculate the impact of present-day clouds in the global warming climate and take the average, which is then the above mentioned two-sided variant. The two-sided diagnostic is given by

$$\left.\frac{\partial T(\phi,p)}{\partial t}\right|_{PRP,average} = \frac{1}{2}\Big[\Big(R(T_{CTL},q_{CTL},c_{WRM}) - R(T_{CTL},q_{CTL},c_{CTL})\Big) - \Big(R(T_{WRM},q_{WRM},c_{CTL}) - R(T_{WRM},q_{WRM},c_{WRM})\Big)\Big]. \quad (4.10)$$

The impact of radiative changes in water vapor is calculated the same way but applied to the variable q.

As already mentioned, the advantage of this method is that differences in the temperature and water vapor distributions between the clear-sky and all-sky atmosphere do not impact the changes in cloud-radiative heating and therefore can be interpreted more easily. This impact is also called cloud masking. The disadvantages of the PRP calculations are on the one hand that their results cannot be compared to measurements and on the other hand that assumptions of linearity and separability are made, e.g., different radiative feedbacks for clouds and water vapor. However, for a modest climate change on a global scale, the influence of nonlinear relationships should be small and different radiative feedbacks should show a high degree of separability (Bony et al., 2006; Soden et al., 2004; Colman et al., 1997).

5. Results and Discussion

We now want to answer the research questions. To this end, we go from a global scale in Question 1 to a regional scale in Question 2. Lastly, we will discuss Question 3 looking into the changes in cloud-radiative heating under global warming and its predictability.

5.1 Question 1

> What is the role of clouds in setting the zonal-mean circulation response to warming on a global scale and how is the cloud impact distributed between the atmospheric and surface pathways?

To begin answering Question 1, we first characterize the general circulation changes in SLAB under global warming in Fig. 5.1. We then use our results from the cloud-locking method for SLAB and SSTSLAB to quantify the zonal-mean circulation response distributed between the atmospheric and surface pathways. At the end of this section, we compare our results to Voigt et al. (2019) and look at the changes in cloud-radiative heating from the PRP calculations, in order to explain different model behaviors.

Starting with the general characterization of the circulation changes in SLAB, the left panel of Fig. 5.1 depicts the impact of the CO_2 increase on the annual-mean zonal-mean temperature ΔT, zonal wind Δu and Hadley cells in terms of the mass stream function $\Delta\psi$. The right panel shows the residuals between the free response and the total locked response. Fig. 5.1a depicts typical features of the global warming impact in coupled atmosphere-ocean models, like an amplified heating in the upper levels of the equatorial and lower levels of the arctic troposphere, as well as a cooling of the stratosphere due to increased stratospheric CO_2 and water vapor (Ceppi and Shepherd, 2017).

In the Southern Hemisphere of Fig. 5.1c at around 200 hPa, we find the previously in

subsection 4.3.1 discussed merged subtropical and midlatitude jet streams. The upward shift of the jet streams in both hemispheres under global warming, is depicted by a strengthening above the jet stream maxima of SLAB-CTL (contours), which indicates the vertical expansion of the troposphere. The dipoles of strengthening throughout the whole atmosphere at around 60°N/S and weakening at around 30°N/S point to the poleward shift of the midlatitude jet streams.

The vertical expansion of the troposphere can also be seen in Fig. 5.1e where the Hadley cells strengthens near the tropopause in both hemispheres. But like mentioned in subsection 4.3.2, Fig. 5.1e also shows no clear edge for the Hadley cell in the Northern Hemisphere and also no clear patterns of the Ferrel cells in NH and SH. This differs from results in Albern et al. (2019) and Voigt et al. (2019) where the NWP-physical package of ICON has been used. Although the Ferrel cell is not visible in the control climate, the strengthening of the negative mass transport (westwards) in the Northern Hemisphere at around 40° to 70° and the strengthening of the positive mass transport (also westwards because of the sign change of the mass stream function in the SH) at around 30° to 60° under global warming could mean an overall increase in the midlatitude storm track activity.

The right panel of Fig. 5.1 shows small residuals for the annual-mean zonal-mean temperature and zonal wind but larger ones (nearly half of the total change locally) for the mass stream function. However, in an annual-mean spatial-mean, the residual for the mass stream function is roughly one quarter (0.1 kg s^{-1}) of the total locked response (0.4 kg s^{-1}) and less for the total free response (0.5 kg s^{-1}). This shows that the cloud-locking method works well for the annual-mean zonal-mean overall response of temperature, zonal wind, and mass stream function to 4xCO_2.

To quantify the zonal-mean response of the atmospheric circulation changes under global warming, and account for the impact of the atmospheric and surface pathways we juxtapose the results from SLAB and SSTSLAB in Fig. 5.2. Fig. 5.2 compares the change in the position of the midlatitude jet streams and the subtropical latitudes of zero net precipitation arising from the total cloud impact in SLAB (atmospheric pathway + surface pathway), with the response from the atmospheric pathway only (SSTSLAB). First we can see that the total free change from SLAB (open black bar), the total locked change from SLAB (cross) and the total locked change from SSTSLAB (star) is fairly close to each other, for the Northern Hemisphere as well as for the Southern Hemisphere. The same is true for the latitude of zero net precipitation. That means that, on a global scale, the cloud-locking method also works well for both circulation metrics. A small residual means, that the simulations agree with each other, and the internal variability as well as decorrelation effects are low.

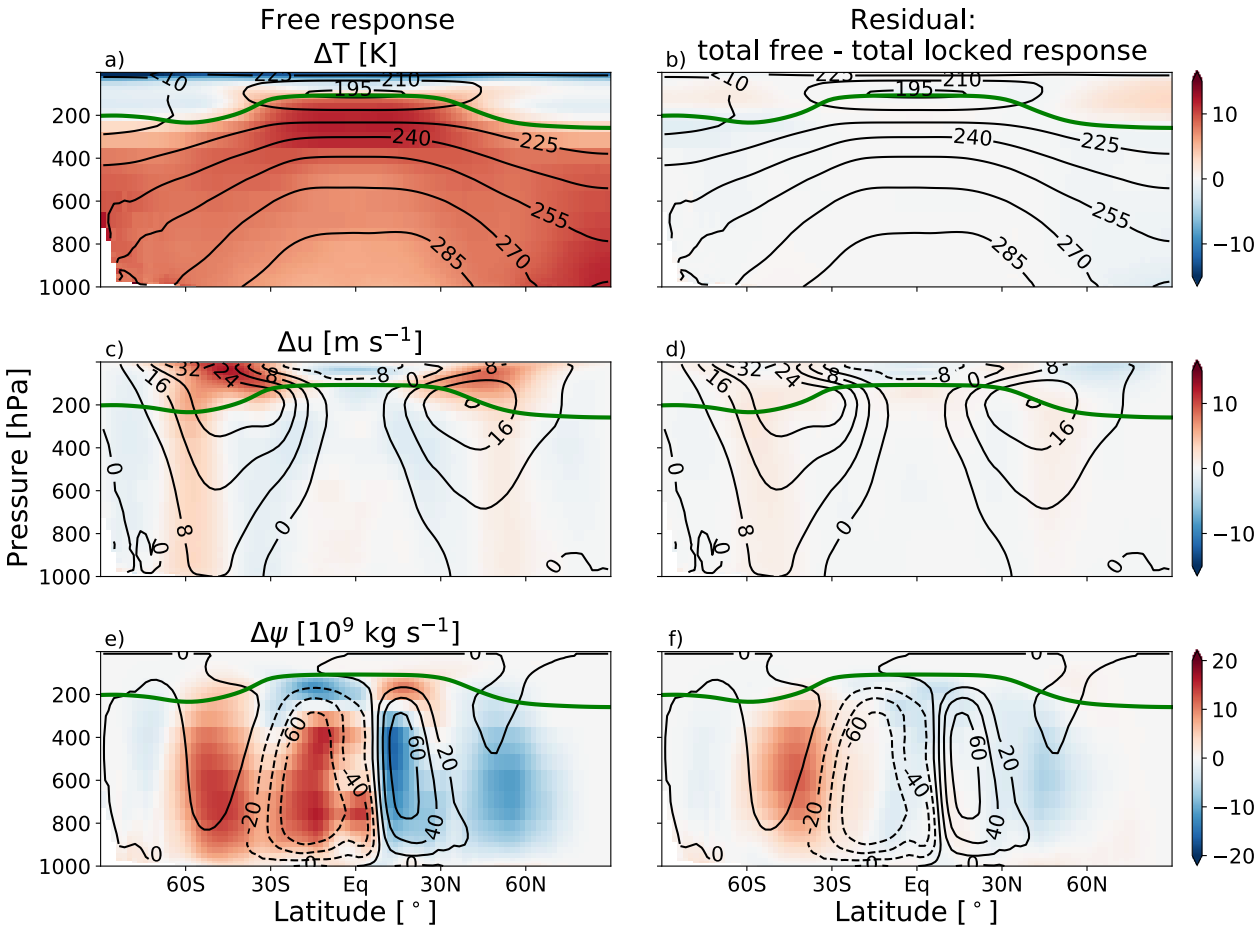

Figure 5.1: Free overall response to a quadrupling of CO_2 (left) and difference between response of free and locked simulations (right) for annual-mean zonal-mean temperature (a-b), zonal wind (c-d), and mass stream function (e-f) in the SLAB simulation set. Colors depict the change in the respective parameters, and contours represent the values for the present-day control simulation. The green line shows the height of the tropopause from SLAB-CTL.

Fig. 5.2a depicts a clear poleward jet shift in both hemispheres for the total response. The total cloud contribution accounts for nearly all of the total response in the Southern Hemisphere and for even more in the Northern Hemisphere, showing the leading role of the cloud impact. Even if the surface pathway is disabled, clouds still account for half of the jet shift under a quadrupling of CO_2 in both hemispheres.

For the subtropical latitude of zero net precipitation (P-E=0) we find a different relationship between the atmospheric and surface pathways than for the jet shift. Although Fig. 5.2b again shows the leading role of the cloud impact, the atmospheric pathway seems less active as for the jet shift. Here, the atmospheric pathway does not account for half of the cloud contribution anymore but less, the surface pathway being dominant.

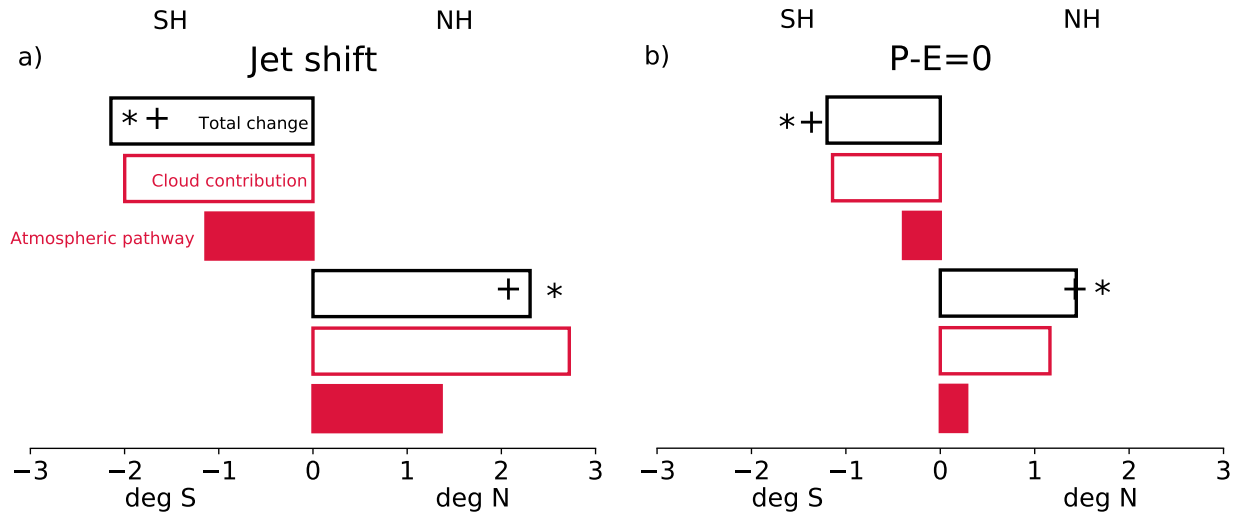

Figure 5.2: Metrics of the global atmospheric circulation change for the Northern Hemisphere (NH) and the Southern Hemisphere (SH). (a) Change in jet latitude and (b) change in the latitude of zero net precipitation. The black bar shows the total free change from the SLAB simulation set under a quadrupling of CO_2. The open red bar shows the total cloud contribution from SLAB and the filled red bar denotes the contribution just from the atmospheric pathway, which is derived from the SSTSLAB simulation set. The stars refer to the total locked response from SSTSLAB and the crosses to the total locked response from SLAB for the respective hemisphere.

Similar importance of the cloud contribution on these circulation metrics in the zonal mean was also found in Voigt et al. (2019), but with a different activity of the atmospheric and surface pathways. In order to explain possible reasons for this difference we now look at the cloud-radiative heating changes under a quadrupling of CO_2 in Fig. 5.3 and compare our results to the results of Voigt et al. (2019).

The cloud-radiative heating changes at TOA are characterized in Fig. 5.3a. We see the change in longwave CRE dominating over the change in shortwave CRE in the tropics and vice versa in the midlatitudes around 45°N/S. This leads to an overall warming of TOA by net cloud-radiative heating, with peaks in the midlatiutes. This means that our results for TOA do not show a large influence of cloud radiative heating on the meridional temperature gradient, whereas cloud radiative heating within the atmosphere and at the surface certainly does.

Within the atmosphere, longwave cloud-radiative heating is more relevant then shortwave cloud-radiative heating. Fig. 5.3b shows the typical arc-shaped pattern of upper tropospheric cloud-radiative heating extending from the tropics to the midlatitudes, also found in many other models (e.g. Voigt et al., 2019). It is accompanied by a reduction of cloud fraction within the areas of heating and an increase above, which represents an upward shift

of the upper tropospheric ice clouds. This arc-shaped pattern of anomalous cloud-radiative heating in the upper troposphere strengthens the meridional equator-to-pole temperature gradient and baroclinicity in the upper troposphere (Fig. 5.1a), supporting the poleward atmospheric circulation shift, which has been found to be a robust response in climate models and acts to enhance the jet response to climate change (Voigt et al., 2019; Li et al., 2019).

The surface cloud-radiative heating is characterized by an anomalous cooling of the equatorial latitudes as well as the southern high latitudes and an anomalous warming of the low latitudes in both hemispheres (Fig. 5.3c). For the vertically integrated atmospheric cloud-radiative heating, a warming effect with maxima in the tropical latitudes and around 60° S, as well as a cooling at high latitudes, can be seen. In the Northern Hemisphere, this translates into an overall increase in baroclinicity, whereas in the Southern Hemisphere, this effect is less pronounced due to the heating maximum at around 60° N. For the net cloud-radiative heating, 5.3c shows the maximum values at the poles, supporting the polar amplification. Except at the poles, the meridional net heating pattern is dominated by shortwave cloud-radiative heating. Because the surface pathway acts by impacting the surface temperature gradient, Fig. 5.3c now allows us to make the connection between the differences in our results and the results from Voigt et al. (2019).

Regarding the jet response to 4xCO_2 in Fig. 5.2a, Voigt et al. (2019) found a dominating role of the atmospheric pathway over the surface pathway in the Northern Hemisphere, whereas our results indicate equal importance. Additionally, in the Southern Hemisphere, our results show a weaker jet shift of about 1° compared to Fig. 5.2a in Voigt et al. (2019). The latter can be explained by an overall weaker cloud-radiative heating of the equatorial upper troposphere in our simulations, and a weaker net cloud-radiative cooling at 60° S by more than one half. As discussed in section 1.1, these are both important mechanisms of clouds strengthening the equator to pool temperature gradient. Regarding the dominating atmospheric pathway for the jet shift in the Northern Hemisphere, Voigt et al. (2019) found a strong impact from longwave cloud changes in the northern high latitudes compared to the cloud-radiative changes in the southern high latitudes. Our results show an overall lower impact of shortwave cloud-radiative cooling in the southern high latitudes. Furthermore, longwave warming and shortwave cooling are more balanced in the northern high latitudes between 60° and 90° than in Voigt et al. (2019), which may lead to an equal importance of the surface and atmospheric pathways for the jet shift in the NH.

Regarding the poleward shift of the subtropical latitude of zero net precipitation, Voigt et al. (2019) found a dominance of the atmospheric pathway over the surface pathway in both hemispheres, whereas our results show the opposite (Fig. 5.2b). This may also be

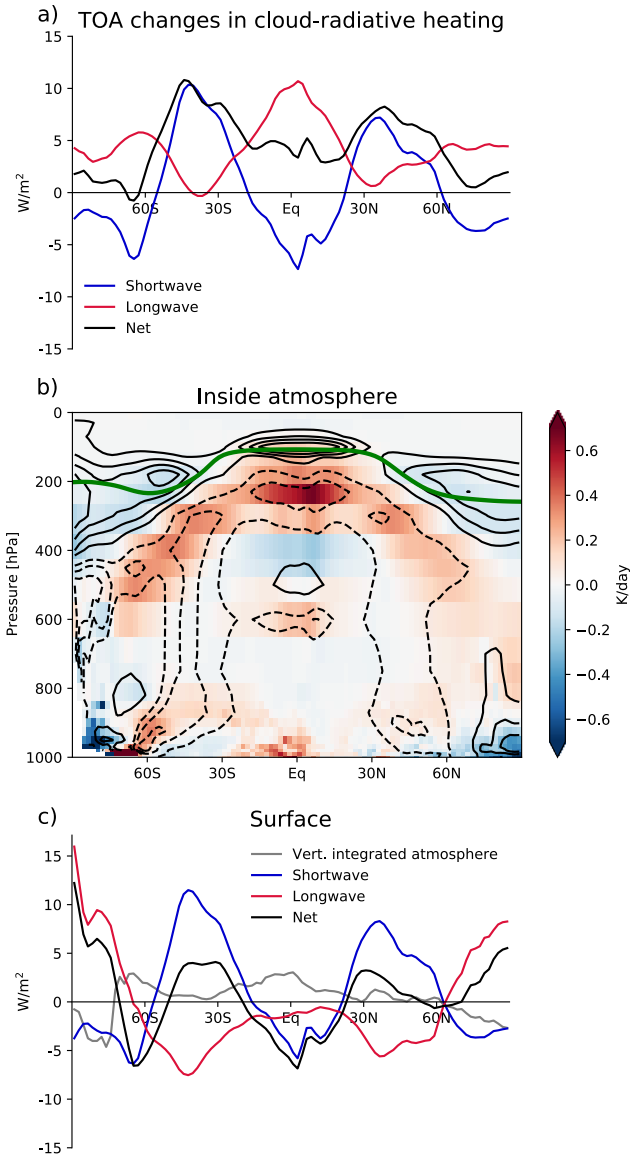

Figure 5.3: Changes in cloud-radiative heating at (a) TOA , (b) inside the atmosphere, and at (c) the surface from the PRP calculation under quadrupling of CO_2 for SLAB. Colors in (b) show the net cloud-radiative heating. Solid contours are positive changes in cloud fraction, and dashed ones are negative changes with intervals of 2%. The green line represents the level of the tropopause from the SLAB-CTL simulation.

explained by the different changes in long and shortwave surface cloud-radiative heating in Fig. 5.3c. We find more distinctly formed dipoles of the shortwave cloud-radiative heating between the low and mid-latitudes, showing clear negative values for the equator. Overall, this may lead to a more effective contribution from the surface pathway to the circulation change under global warming. A further possible explanation of the surface pathway dominating over the atmospheric pathway in our results may also be the less pronounced changes in Hadley cell edges. If changes in subtropical drying effects, caused by strong subsidence of the descending branch of the Hadley cells are less pronounced, they have a weaker influence on circulation changes which in turn would strengthen the relative influence of changes in transient eddies and midlatitude storm tracks (Fig. 5.1e). Because the surface pathway is likely dominated by low-level clouds, this may results in a stronger activity of the surface pathway compared to the atmospheric pathway.

To answer Question 1, we summarize our results for the relative roles of the atmospheric and surface pathways on the zonal-mean circulation response in the Northern and Southern Hemisphere:

1. Like previous studies, we found a poleward circulation expansion and a vertical expansion of the troposphere in the zonal mean for the Northern and Southern Hemispheres under global warming (Figs. 5.1c, 5.1e, and 5.2). Fig. 5.2 shows that cloud-radiative changes account for nearly all of the total poleward jet shift and the poleward shift of the subtropical latitude of zero net precipitation in our simulations in both hemispheres.

2. For the jet shift, the impact of the atmospheric pathway is roughly equal to the impact of the surface pathway. For the polewards shift of the subtropical latitude of zero net precipitation the surface pathway is dominating.

3. The reason for the different relative importance of the atmospheric and surface pathways in our simulation compared to results of Voigt et al. (2019), is due to the different responses of the short and longwave cloud-radiatve heating changes to $4xCO_2$.

4. In the zonal mean, the cloud-locking method works well. Not only is the residual for ΔT, Δu and $\Delta\psi$ in Figs. 5.1b, 5.1d, and 5.1f, small, but also the differences between the locked and free responses of the circulation metrics in SLAB and SSTSLAB (Figs. 5.2a and 5.2b).

5.2 Question 2

> Focusing on the three ocean basins of the North Atlantic, North Pacific, and Southern Hemisphere, what is the relative role of the atmospheric and surface pathways in the jet response regionally?

To answer Question 2, we will have a closer look at the impact of the atmospheric and surface pathways on the regional change of the atmospheric circulation under global warming, focusing on the three main ocean basins: the North Atlantic, the North Pacific, and the Southern Hemisphere ocean basin.

But first, to get a better sense of the overall pattern of the cloud impact in the single ocean basins, we will have a look at the annual-mean zonal wind response to warming at the 850 hPa level (u_{850}). In order to do that, we decompose the u_{850} response into the total

response, the cloud-radiative impact, the water vapor impact, and the impact of changes in CO_2/SST without any changes in clouds and water vapor. After this, we will focus on the zonal-mean zonal wind response in the single ocean basins.

5.2.1 Annual-Mean Response of u_{850}

In order to account for the pattern of the cloud impact on u_{850}, divided into the atmospheric and surface pathways, we again juxtapose the results for SLAB and SSTSLAB. The total response for SLAB and SSTSLAB in Fig. 5.4a and 5.4b shows a significant poleward shift of the jet latitude for nearly all longitudes in both hemispheres, except over Russia and Asia. This is not of concern because we are interested in the ocean basins, where, because of the low friction, the jet stream is normally defined. The 95% (p=0.05) significance level for each grid point in Fig. 5.4 and Fig. 5.5 is calculated with a two-sample t test, similar to Albern et al. (2019). One sample for the t test is the decomposed annual-mean responses of u_{850} from the locked simulation sets and the other sample is the total free annual-mean responses of the respective CTL and WRM simulation sets. If both samples are statistically similar at a 95% significance level, we mark the grid point with a dot.

In the central and eastern South Pacific, Figs. 5.4a and 5.4b show a strengthening rather than a poleward shift. The poleward shift can be seen by a dipole of a weakening of u_{850} equatorwards of the jet latitude and a strengthening polewards of the jet latitude. A significant dipole of strengthening and weakening is found in the North and South Atlantic, the Indian Ocean, and the eastern North Pacific. In the western North Pacific, the total response does not show a significant weakening equatorwards of the jet latitude.

Fig. 5.4c shows the atmospheric pathway of the cloud impact (SSTSLAB) and the combined effect of the atmospheric and surface pathways (SLAB) is shown in Fig. 5.4d. The combined effect of the atmospheric and surface pathways can be seen in the overall increased magnitude of the cloud impact for SLAB. Because the SSTs are prescribed to the SLAB climatology in SSTSLAB they can not react to changes in cloud-radiative heating, which means that the surface pathway is disabled. Consequently the overall magnitude of the cloud impact decrease. This decrease in the cloud impact is partly taken over by the SST impact in SSTSLAB, which can be seen by comparing Fig. 5.4g with Fig. 5.4h. By prescribing SST in SSTSLAB we also effect water vapor in the atmosphere. Because SSTs can not change due to changes in cloud radiation in SSTSLAB, where they can change in SLAB, the pattern of the isolated water vapor impact is also different (Fig. 5.4e and 5.4f).

Overall, the total response as well as the cloud impact show a very zonally symmetric pattern around the jet latitude for both SSTSLAB and SLAB. Clouds even depict a significant

impact for the entire North Pacific, whereas the total locked response does not. Because both the cloud impact in Fig. 5.4c and 5.4d show this symmetry around the jet latitude, we can conclude that the surface pathway, which is Fig. 5.4c subtracted from Fig. 5.4d, must be symmetric around the jet latitude too.

Water vapor and SST/CO_2 for both simulation sets does not show the same symmetric behavior of a significant poleward jet shift. Water vapor even depicts a somewhat clear equatorward shift for the North Pacific and SH in SLAB and the SH in SSTSLAB. This means that clouds really contribute most to the zonally symmetric jet shift we find for the total response.

To be able to compare ICON-ESM under the same experimental setup as used in Albern et al. (2019) with the NWP physics package, Fig. 5.5 shows the impact on u_{850} for a uniform SST increase of 4 K, as described in subsection 4.2.1.

If we compare the total locked response on u_{850} in Fig. 5.5 to Figs. 5.4a and 5.4b, the most prominent difference arises from the strong equatorward jet shift in the North Pacific. If we look at the SST impact in Fig. 5.5d we can see that this nearly completely comes from the change in SST where the impact of clouds and water vapor is negligible. This shows that when switching from a simulation setup with a CO_2 increase to an increase in SST, where additionally the sea ice cover does not change, the impact strongly shifts from changes in clouds and water vapor to changes in SSTs, and the impact on the jet latitude changes drastically in the NH. Overall, Fig. 5.5a shows that SSTCLIM is not able to reproduce the results for the jet shift in the North Pacific from SLAB or SSTSLAB.

However, Fig. 5.5 depicts the same zonal symmetry for clouds as in Albern et al. (2019) and for our results with SSTSLAB and SLAB in Fig. 5.4, even if not quite as strong or significant as our results for SSTSLAB and SLAB. That means that although there are huge overall discrepancies in the total impact from one simulation to another and also from one model version to another, the cloud impact does show a robust poleward jet shift, which is a reliable model feature in our results and across different experiments regarding the changes in the atmospheric circulation.

The water vapor impact of SSTCLIM in Fig. 5.5c is also in line with the results for the significant jet response in SSTSLAB and SLAB, showing a jet strengthening in the two NH ocean basins and an equatorward shift in the SH. For the water vapor impact, no comparison can be made to Albern et al. (2019) since in Albern et al. (2019) it was not evaluated.

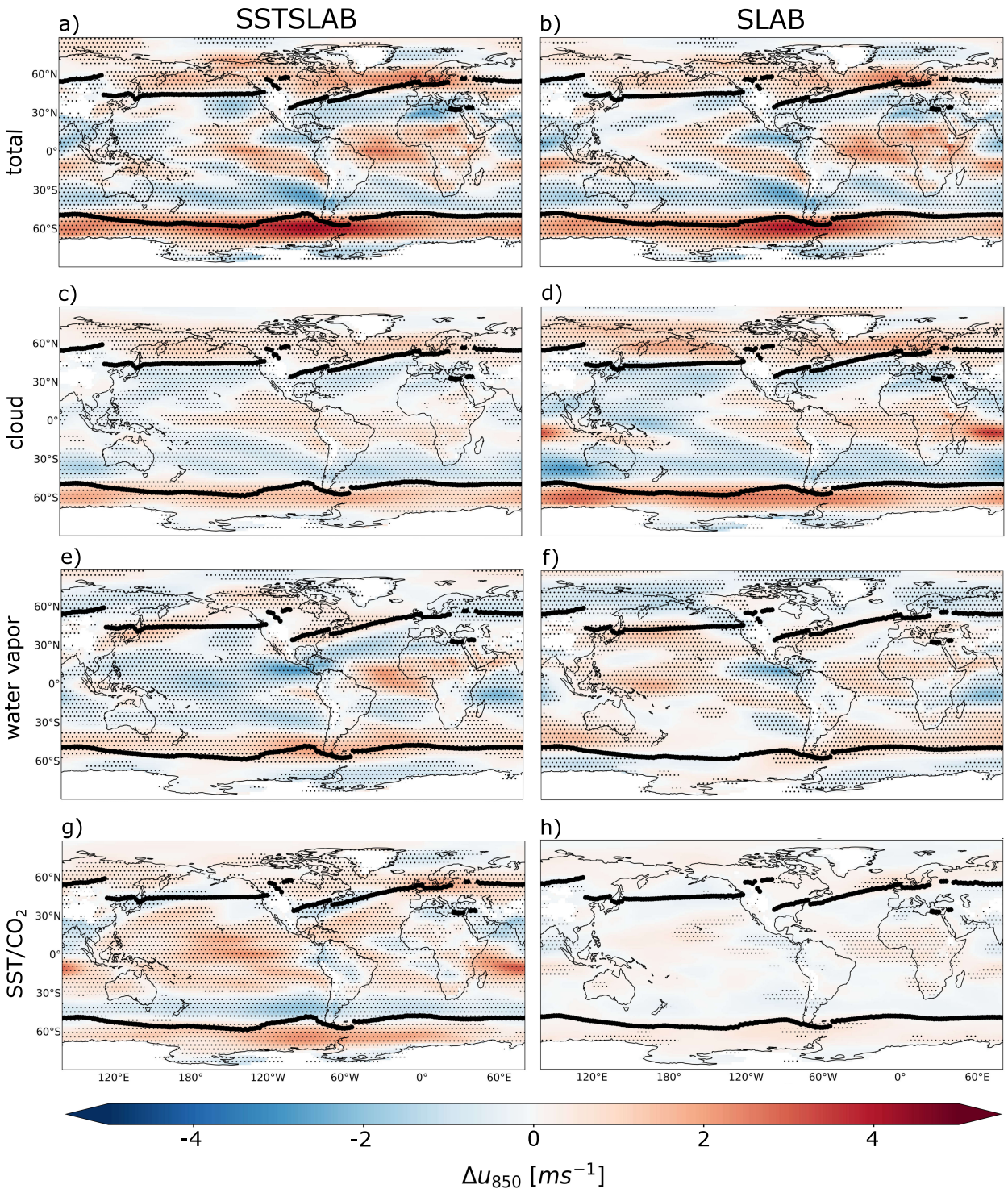

Figure 5.4: Annual-mean response of the 850-hPa zonal wind u_{850} for the SSTSLAB simulation set (left) and the SLAB simulation set (right). The response is decomposed into the total locked response (a,b), the cloud impact (c,d), the water vapor impact (e,f) and the SST/CO_2 impact without changes in clouds or water vapor (g,h). The last figure in the left column shows the impact of changes in SST only (g) and the last figure in the right column shows the impact of changes in CO_2 only (h). The black lines indicate the jet latitude from SSTSLAB-CTL (left) and SLAB-CTL (right). Dots show where the response is 95% significant.

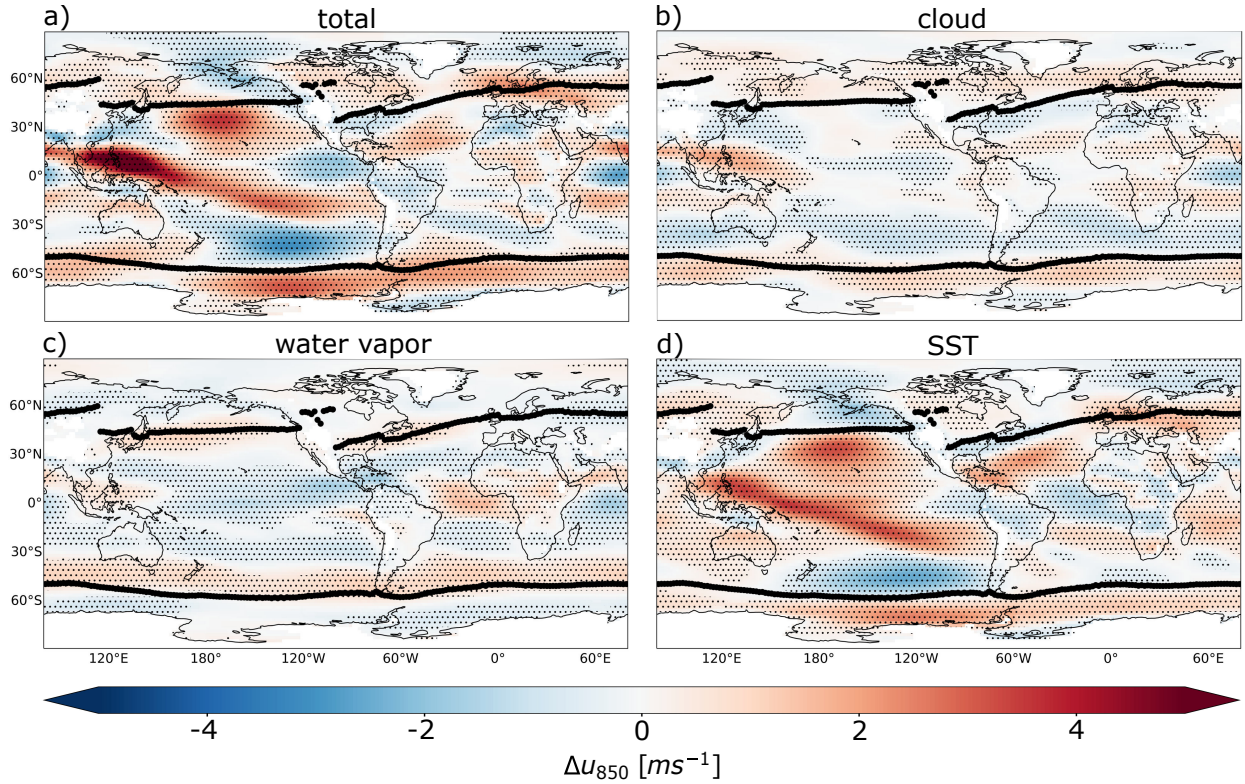

Figure 5.5: Annual-mean response of the 850-hPa zonal wind u_{850} for the SSTCLIM simulation set. The response is decomposed into the total locked response (a), the cloud impact (b), the water vapor impact (c) and the SST impact without changes in clouds or water vapor (d). The black lines indicate the jet latitude from SSTCLIM-CTL. Dots show where the response is 95% significant.

We have seen that, on a global scale, as in Albern et al. (2019) and Voigt et al. (2019), the poleward shift is mostly caused by clouds, even when the surface pathway is turned off and the pattern of the cloud impact is zonally symmetric around the jet latitude for the atmospheric pathway and the surface pathway. In our results for SSTCLIM, an equatorward jet shift is found for the North Pacific, which is dominated by changes in SSTs. For the same simulation setup, Albern et al. (2019) found a poleward jet shift in the North Pacific.

5.2.2 Annual-Mean Zonal-Mean Response of u_{850} for Single Ocean Basins

Following Albern et al. (2019), we now look at the annual-mean zonal-mean decomposed response of u_{850} under global warming in the three main ocean basins. Having discussed the qualitative impact of clouds on jet streams in each ocean basin in the previous section, this allows us to quantify the total locked jet response and its decomposition on a regional scale.

The total locked response for SLAB in Fig. 5.6 (left panel) depicts the clear poleward jet shift in all three ocean basins by showing the dipole between the strengthening of u_{850}

polewards of the jet latitude, which is obtained from SLAB-CTL (gray vertical bar), and a weakening equatorwards. This is in line with our findings for SLAB in the previous chapter.

The left panel in Fig. 5.6 also shows a qualitative agreement between the total locked (black line) and the free response (gray line) of SLAB. But the quantification of the jet shift in the right panel, shows that the total locked response is at roughly 4.5°, where the free response of the jet shift is just approximately 2.5°. Thus, the cloud-locking method overestimates the jet shift in the North Atlantic by about 2°. However, the jet strengthening in the North Atlantic is well captured by the cloud-locking method, showing an increase of 1.2 m s^{-1}. Exact values of all responses are presented in Fig. A.1 of the Appendix.

Similar results can be found for the North Pacific. Here Fig. 5.6 shows a total locked response of the jet shift of about 1° and a free response of nearly 2°. Hence, an underestimation of the cloud-locking method by approximately one degree, which is about half of the total free response. The strengthening of the jet ($\approx$ 0.5 m s^{-1}) in the North Pacific is much less than in the North Atlantic.

For the SH, the total locked response as well as the free response is around two degrees for the jet latitude and around 2.5 m s^{-1} for the jet strength, showing a small residual. In combination with our results in Fig. 5.2, where the difference between the total locked and free response for the entire zonal mean of the Northern Hemisphere is also small, we can conclude that while the cloud-locking method works well on a global scale, the residuals on a regional scale, in terms of the North Atlantic and North Pacific, increase strongly.

Having a closer look at the right panel of Fig. 5.6, we quantify that clouds contribute most to the jet shift of the total locked response in all three ocean basins. For the North Atlantic, the cloud impact even exceeds the total free response in terms of the jet shift. Regarding the jet strengthening, in the SH, we find an increase of 1.2 m s^{-1} through cloud-radiative changes, a strengthening of 0.7 m s^{-1} in the North Atlantic, but no strengthening in the North Pacific.

Overall, this confirms the importance of the cloud impact for the combined activity of the atmospheric and surface pathways in the SLAB simulation set on a regional scale. But because the residuals are nearly half of the total free response for the North Atlantic as well as the North Pacific, the magnitude of the total response as well as the decomposed impact needs to be taken with caution. Although the residuals are that big, all four simulation pairs for the jet shift do agree about the sign of the cloud impact. Because of internal model variability and the decorrelation effects of the cloud-locking method as discussed in section

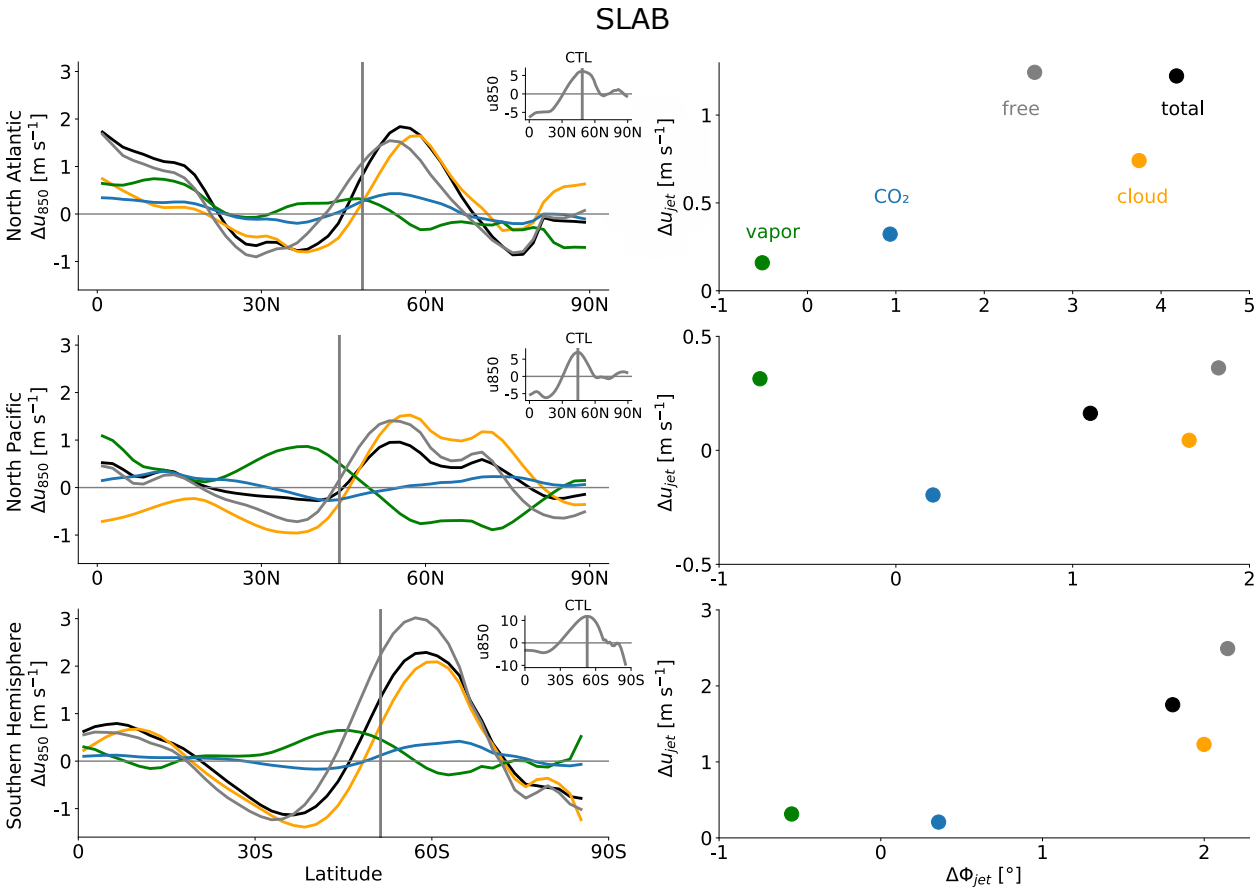

Figure 5.6: Annual-mean zonal-mean response of u_{850} for single ocean basins in the SLAB simulation set (left) and the change in jet latitude and strength for the respective ocean basins (right). Results are shown for the North Atlantic (top), the North Pacific (middle), and the Southern Hemisphere ocean basin (bottom). The gray bars in the left panel depict the jet latitude from the free control simulation. u_{850} from the free control simulation is shown in the upper right corners of the left panel as little inserts. The total locked response (black) in both panels is decomposed into the water vapor (blue), cloud (orange) and SST/CO_2 impact (green). The free response where no radiative properties are locked is shown as gray lines (left) and dots (right).

4.4, if many simulation pairs show the same sign of the jet shift, high certainty about how clouds affect the direction of the jet response is expressed in the simulations. The sign of all the simulation pairs for the decomposed parameters can be seen in the Appendix (Fig. A.1).

If we now look at the SSTSLAB simulation set in Fig. 5.7 in order to isolate the atmospheric pathway, we can quantify the reduction of the cloud impact in the case of the surface pathway being switched off. The total locked response in Fig. 5.7 still shows a clear dipole of jet strengthening polewards of the jet latitude and a weakening equatorwards (left panel), but the cloud-radiative impact in the North Atlantic and the SH decreases to approximately one half of the total locked response. Compared to SLAB the cloud impact in the North Pacific

decreases too, but they still account for nearly all of the total jet response. For the North Atlantic, the magnitudes of the cloud impact and the SST/CO_2 impact are equal now, which can be seen in Fig. 5.7 right panel and in the Appendix (Fig. A.2). Fig. 5.7 also shows a more equal magnitude of cloud impact and SST/CO_2 impact for the SH compared to the SLAB simulation set.

Interestingly, the residual for the North Pacific reduces strongly in SSTSLAB compared to SLAB, where it does not change in magnitude for the North Atlantic. But this decreased residual for the North Pacific arises from an overall reduced free response, because the total locked response stays the same at about 1.1° in SLAB and SSTSLAB. This can be seen by comparing the right panel of Fig. 5.7 with Fig. 5.6.

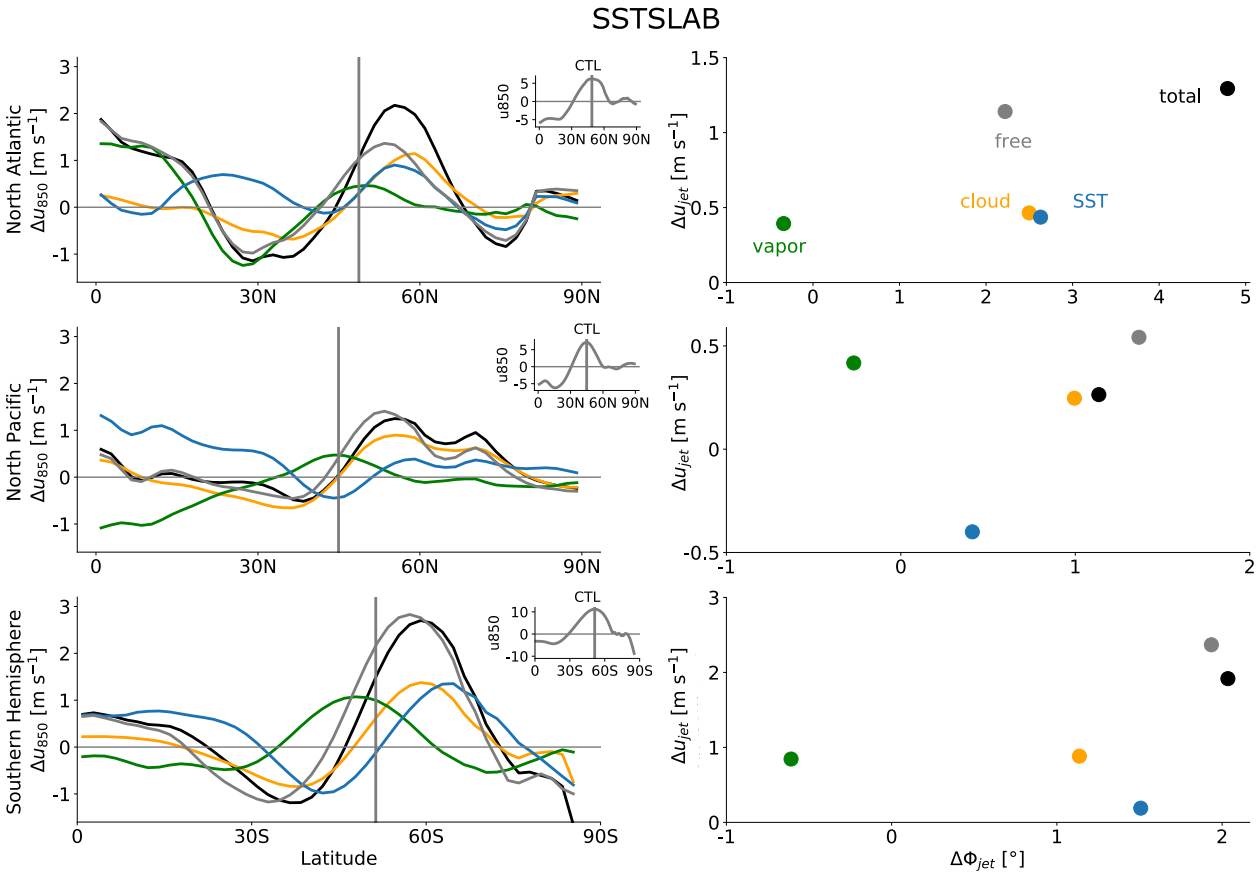

Figure 5.7: Annual-mean zonal-mean response of u_{850} for single ocean basins in the SSTSLAB simulation set (left) and the change in jet latitude and strength for the respective ocean basins (right). Results are shown for the North Atlantic (top), the North Pacific (middle), and the Southern Hemisphere ocean basin (bottom). The gray bars in the left panel depict the jet latitude from the free control simulation. u_{850} from the free control simulation is shown in the upper right corners of the left panel as little inserts. The total locked response (black) in both panels is decomposed into the water vapor (blue), cloud (orange) and SST/CO_2 impact (green). The free response where no radiative properties are locked is shown as gray lines (left) and dots (right).

To establish the connection between our results and the work of Albern et al. (2019) we repeat this analysis also for the SSTCLIM simulation set. As we saw the equatorward jet shift in the North Pacific in Fig. 5.5a, for the total locked response, Fig. 5.8 now lets us quantify this behavior. The second row in Fig. 5.8 shows an equatorward jet shift of 0.7° for the North Pacific (black dot, right panel). The left panel of Fig. 5.8 shows that the total response (black line) is dominated from the SST impact (blue line) which confirms the pattern we saw in Fig. 5.5d. But because the free response of 1.1° (gray dot, right panel) for the North Pacific is negative too, the residual between the locked response and the free response is moderate ($\approx 0.4°$).

According to the equatorward jet shift, the jet strengthening in SSTCLIM (0.6 m s^{-1}) is stronger for the North Pacific than in SLAB (0.2 m s^{-1}) and SSTSLAB (0.3 m s^{-1}) even if it undergoes a smaller global warming of the surface temperature.

Looking at the cloud impact in SSTCLIM, we find that they again contribute to a poleward jet shift in all ocean basins. Furthermore, the cloud impact robustly agree on the sign of the jet shift in all simulation pairs of the cloud-locking method across all ocean basins, which can be seen in the Fig. A.3 of the Appendix. In the North Atlantic and the Southern Hemisphere clouds account for nearly all of the total locked poleward jet shifts of 1.8° and 0.9°, respectively.

Compared to Albern et al. (2019), the model behavior of ICON for the North Pacific changed quite strongly. Whereas in our results we find an equatorward jet shift of 0.7°, Fig. 6 of Albern et al. (2019) shows a poleward jet shift in the North Pacific of about 2.2°. That could be due to a stronger activity of the shortwave near surface CRE and thus an enhanced warming of the Arctic lower troposphere in SSTCLIM compared to the simulations of Albern et al. (2019). This would act to reduce the surface pole-to-equator temperature gradient in the Northern Hemisphere, which complicates things and can lead to this behavior in model experiments (Butler et al., 2010; Grise and Polvani, 2014, Fig. 3, right column for "SSTs only", first row). But this is just an assumption because we did not calculate the changes in shortwave and longwave fluxes for this simulation set.

Concerning the SH, the total impact compares well to Albern et al. (2019), with a slight increase in the cloud impact. The total impact on the jet shift for the North Atlantic is reduced to 2° in our simulations instead of 4° in Albern et al. (2019).

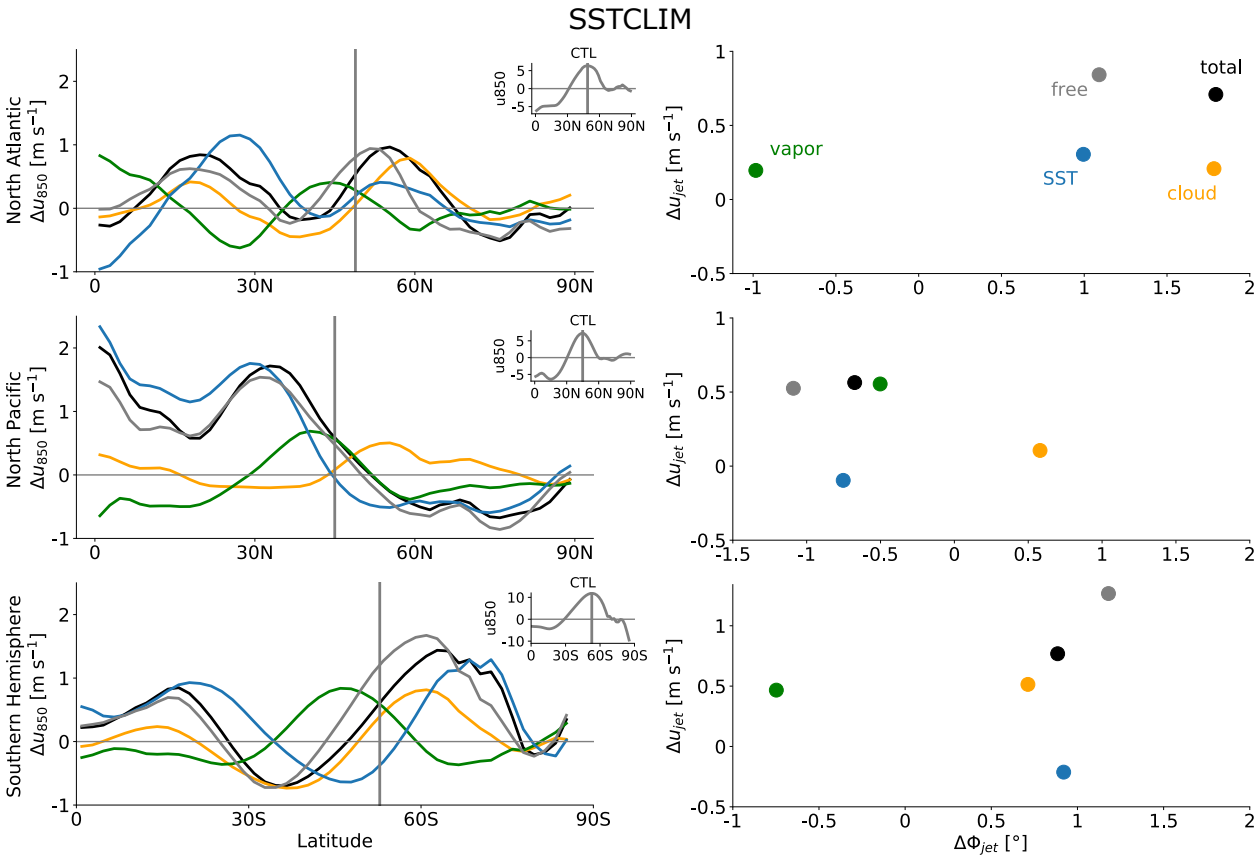

Figure 5.8: Annual-mean zonal-mean response of u_{850} for single ocean basins in the SSTCLIM simulation set (left) and the change in jet latitude and strength for the respective ocean basins (right). Results are shown for the North Atlantic (top), the North Pacific (middle), and the Southern Hemisphere ocean basin (bottom). The gray bars in the left panel depict the jet latitude from the free control simulation. u_{850} from the free control simulation is shown in the upper right corners of the left panel as little inserts. The total locked response (black) in both panels is decomposed into the water vapor (blue), cloud (orange) and SST/CO_2 impact (green). The free response where no radiative properties are locked is shown as gray lines (left) and dots (right).

In order to answer Question 2, we will summarize our findings:

1. The cloud impact is robustly responsible for a large part of the poleward jet shift across all simulation setups and also in all three ocean basins. The patterns of the atmospheric and surface pathways are zonally symmetric around the jet latitude everywhere in the NH and nearly everywhere in the SH (Figs. 5.4c, 5.4d, and 5.5b).

2. Under a quadrupling of CO_2, the atmospheric pathway accounts for half of the jet shift in the North Atlantic and the SH and for all of the jet shift in the North Pacific (Fig. 5.7). Under a uniform 4-K SST increase, clouds still support a poleward jet shift, whereas the total locked response of the jet stream is equatorwards (Fig. 5.8).

3. The overall behavior of ICON-ESM version 2.6.2.2 with the climate physics package

changed strongly for the North Pacific, compared to the work of Albern et al. (2019). This may be because of a stronger polar amplification in our simulations for SSTCLIM.

4. The residual between the total locked response and free response does increase strongly on a regional scale for both of the NH ocean basins. Because of that, the magnitude of the jet shift needs to be taken with caution on a regional level. But because the signs of the free response and the total locked response are the same, the direction of the jet shift can be trusted.

5. Overall, the jet shift in the North Atlantic for a quadrupling of CO_2 is much more pronounced than in the North Pacific and in the SH.

6. Significant jet strengthening can be found in the North Atlantic and the Southern Hemisphere under a quadrupling of CO_2. Clouds account for two thirds of the total locked strengthening of 1.2 m s^{-1} in the North Atlantic and for the total locked strengthening of 1.8 m s^{-1} in the SH. When the surface pathway is switched off, they still account for nearly half of the total jet strengthening in these two ocean basins. For the North Pacific, the total locked strengthening under quadrupling of CO_2 is found to be much smaller (0.2 m s^{-1}).

5.3 Question 3

What are the changes in cloud-radiative heating in ICON-ESM under global warming, and are these changes captured by an upward shift of the present-day cloud-radiative heating?

In Voigt et al. (2019) a large difference in the magnitude of the arc-shaped upper-tropospheric cloud-radiative heating pattern across three models under a uniform 4-K SST increase has been found for the atmospheric pathway. The arc-shaped pattern in the models, studied from Voigt et al. (2019) was qualitatively similar to what we saw in Fig. 5.3b. They also showed how the differences in present-day cloud-radiative heating translate into differences in cloud-radiative heating changes under global warming with the help of the upward shift framework derived in Singh and O'Gorman (2012). We now want to repeat the analysis conducted for the three models in Voigt et al. (2019).

To answer Question 3, we will look at the present day cloud-radiative heating in our simulations and compare them to actual measurements from *CloudSat/CALIPSO*. We will also see

how the cloud-radiative heating changes under global warming as calculated from the radiative fluxes (Eq. 1.7) compares to the results of the PRP calculations. Then we will compare our results for the PRP calculations with the results from Voigt et al. (2019) to examine the robustness of the upward shift as applied to the upper-tropospheric cloud-radiative heating. A robust upward shift is considered if the results from Voigt et al. (2019) can be reproduced and ICON-ESM is able to capture the cloud-radiative heating changes under global warming by an upward shift of the present day cloud-radiative heating.

5.3.1 Cloud-Radiative Heating from Radiative Fluxes in SLAB and the Upward Shift Framework

Because the upward shift mainly works through the robust rise of high-level tropical and midlatitude clouds, we are only interested in the troposphere above 500 hPa. With a global mean warming of approximately 7 K at the 850 hPa level in SLAB, we get a β parameter of 1.28, which we round to $\beta = 1.3$ (Eq. 4.8). The upward shifted present-day cloud-radiative heating is evaluated at βp, and in order to diagnose the cloud-radiative heating changes under global warming, the present-day cloud-radiative heating at p is then subtracted from it (dashed lines in Figs. 5.9c and 5.9d).

But to start, we will compare the vertical profiles of the cloud-radiative heating in the present-day climate (CTL, solid line) and the global warming simulation (WRM, dashed line) in Fig. 5.9, which is depicted for (a) the tropics and (b) the midlatitudes, with the results from the three models used in Voigt et al. (2019).

If we look at the upper row in Fig. 5.9 we see a maximum for the cloud-radiative heating in the tropics at around 400 hPa for the CTL simulation and at around 300 hPa for the WRM simulation, a first hint of the upward shift of the upper tropospheric cloud-radiative heating in this region. The same behavior can be found for the heating below the tropopause at around 100 hPa. In the midlatitudes, a dipole of warming can be seen, with a maximum of 0.1 K day^{-1} below 400 hPa and cooling above 400 hPa, with a minimum of around -0.1 K day^{-1} in the present-day simulation. For the global warming simulation in the midlatitudes, the same pattern is shifted to slightly higher altitudes with an increase in the heating maximum to around 0.2 K day^{-1} and a slight decrease in the cooling at around tropopause level. From these results, we expect that the upward shift should work quite well.

And indeed, Fig. 5.9c and 5.9d confirm this expectation. Here we can find that above 500 hPa, the solid line, which now shows the upward shifted present-day cloud-radiative heating changes from Fig. 5.9a and 5.9b, matches the dashed line above 500 hPa, which is

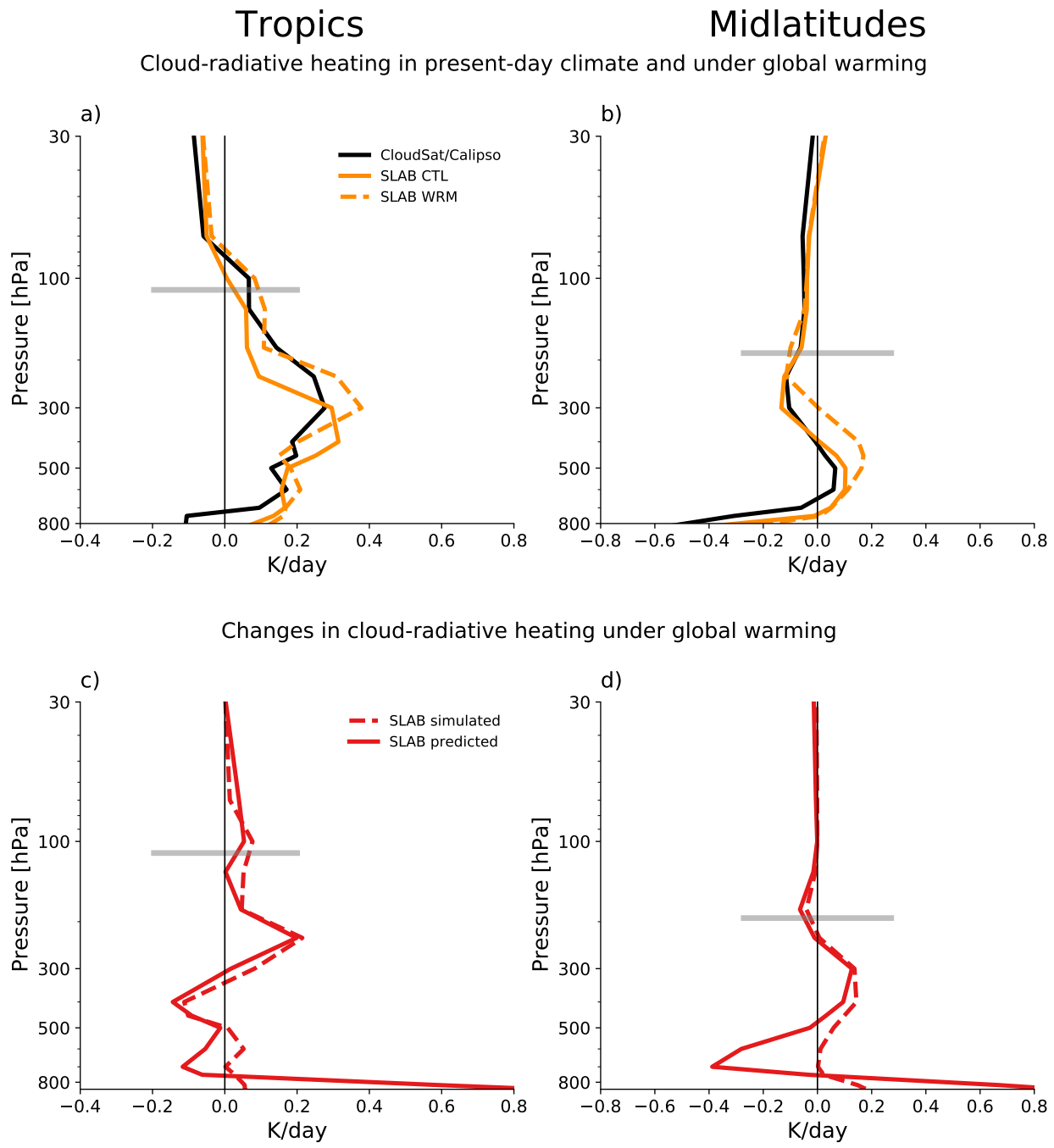

Figure 5.9: (top) Vertical profile of cloud-radiative heating in the SLAB simulation set with a thermodynamic slab ocean for the present-day climate (solid orange line) and under a quadrupling of CO_2 (dashed orange line) for (a) the tropics, which is the average over 30°N-30°S and (b) the midlatitudes, which is the average over 30°-60°N and 30°-60°S. The black solid line shows the present-day cloud-radiative heating from CloudSat/CALIPSO observations, the same as used in Voigt et al. (2019). (bottom) The vertical profile of the cloud-radiative heating changes predicted by the upward shift of the present-day cloud-radiative heating of (a) and (b) (dashed lines) and cloud-radiative heating changes simulated (WRM-CTL, solid line) for (c) the tropics and (d) the midlatitudes. The cloud-radiative heating is calculated from the radiative fluxes and is defined as all-sky minus clear-sky as described in subsection 1.1.1. The gray horizontal bars represent the height of the tropopause in the CTL simulation.

the cloud-radiative heating from CTL minus the cloud-radiative heating from WRM, quite closely. Compared to the results from the PRP calculations in Fig. 8a and Fig. 8b of Voigt et al. (2019) where the same method has been applied for the ICON model version 2.1.00 with a uniform 4-K SST increase and with the physics package used for numerical weather prediction, the upward shift framework works better for the ICON model version 2.6.2.2 coupled to a slab ocean and with the climate physics package.

In Voigt et al. (2019) the upward shift was able to reproduce the pattern of the cloud-radiative heating changes under global warming in the midlatitudes for all three climate models, but for the tropics, this did not work for ICON. It was discovered that ICON's inability, as used in Voigt et al. (2019), was caused by a significant increase in cloud ice due to global warming in the tropical upper troposphere.

To compare this outcome with our results, Fig. 5.10 shows cloud ice and cloud fraction in ICON for the SLAB simulation set as an average for the tropics and the midlatitudes. Following Voigt et al. (2019), both quantities are plotted against temperature because this way, the effects of the expanding troposphere can be take into account. The outcome of this can be seen if we compare Fig. 5.10 with Fig. 5.11, where cloud ice and cloud fraction are plotted against pressure.

Looking at the tropics in Fig. 5.10, cloud ice in our simulations does not show such a huge increase under a global warming scenario anymore relative to the total increase from around 0.004 g kg^{-1} in Voigt et al. (2019) to around 0.015 g kg^{-1}. Cloud ice also increased strongly in the midlatitudes, from approximately 0.004 g kg^{-1} in the simulations of Voigt et al. (2019) to 0.014 g kg^{-1} in our simulations. In the midlatitudes, cloud ice shows no sign of an increase under global warming, whereas cloud fraction decreases because clouds get shifted poleward with the poleward circulation expansion. Cloud fraction in the midlatitudes of ICON-ESM now resembles the results for MPI-ESM in Voigt et al. (2019). Here the same origin of the model physics (ECHAM) comes to light. Cloud fraction in the tropics increases from 5% to 10% between 280 K and 250 K compared to ICON in Voigt et al. (2019), but it does not change much otherwise.

Concentrating now on the comparison of the present-day cloud-radiative heating from our simulations to the measurements taken by *CloudSat/CALIPSO*, Fig. 5.9b shows good agreement in the midlatitudes. For the tropics the maxima does roughly agree on the magnitude of approximately 0.3 K day^{-1}, but the maximum from SLAB-CTL (solid orange line) is slightly shifted downwards from 300 hPa to 400 hPa compared to *CloudSat/CALIPSO* (black line). Overall the vertical profile of cloud-radiative heating in ICON-ESM resembles the qualita-

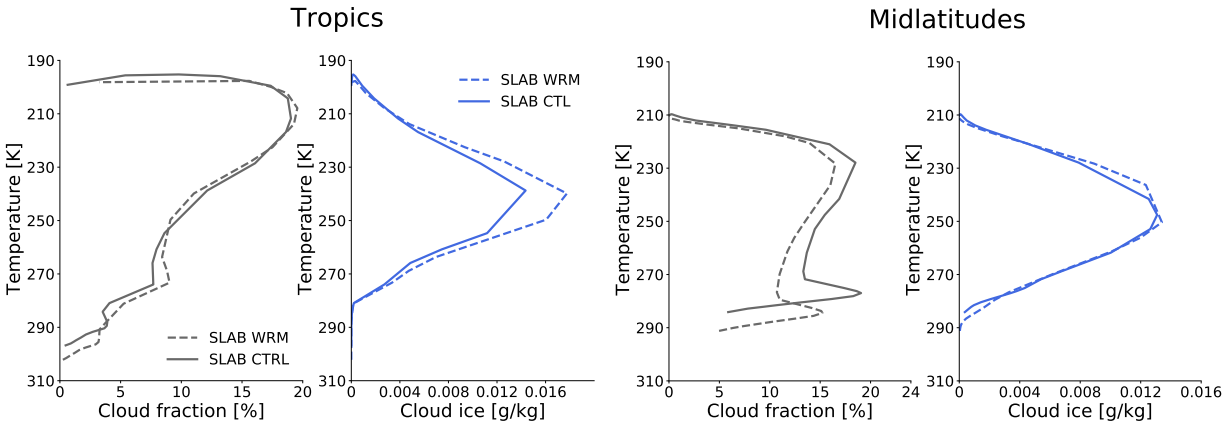

Figure 5.10: Vertical profile of cloud fraction and cloud ice as a function of temperature for the SLAB simulation set under a quadrupling of CO_2 (WRM, dashed) and for the control simulation with 1xCO_2 (CTL, solid) for tropics (left) and midlatitudes (right). The values are averaged over 30°N-30°S for the tropics and over 30°-60°N and 30°-60°S for the midlatitudes.

tive pattern taken by measurements from *CloudSat/CALIPSO* but with quite significant discrepancies. Actually, between 200 hPa and 500 hPa the results from the global warming simulations (dashed orange line) does agree better with the pattern of the vertical profile from *CloudSat/CALIPSO*, except for a higher maximum of 0.4 K day^{-1}.

Nevertheless, the overall profile of the present-day cloud-radiative heating in Fig. 5.9a compares much better with the vertical profile of the measurements taken by *CloudSat/CALIPSO* than most models in Voigt et al. (2019). For example IPSL-CM5A has a maximum of 0.8 K day^{-1} at around 300 hPa, the maximum of ICON, as used as in Voigt et al. (2019), is more than 0.4 at around 200 hPa, and the maximum of the MPI-ESM is nearly 0.4 at around 400 hPa, with a sharp decrease afterwards to a local minimum of 0 K day^{-1} heating just above 300 hPa.

Not even the reanalysis ERA-Interim, shown in Voigt et al. (2019), was able to represent the present-day cloud-radiative heating well. ERA-Interim constrains a numerical weather prediction model through data assimilation of observations and therefore is typically expected to perform better. But because ERA-Interim does not show an improvement in contrast to the models, and because no observations of clouds are considered in ERA-Interim, the problem arises through cloud parametrization.

In the midlatitudes, all models in Voigt et al. (2019) were able to capture the heating dipole depicted in Fig. 5.9b qualitatively, except IPSL-CM5A. But also in the midlatitudes, ICON-ESM shows a better agreement with *CloudSat/CALIPSO* than all the other models.

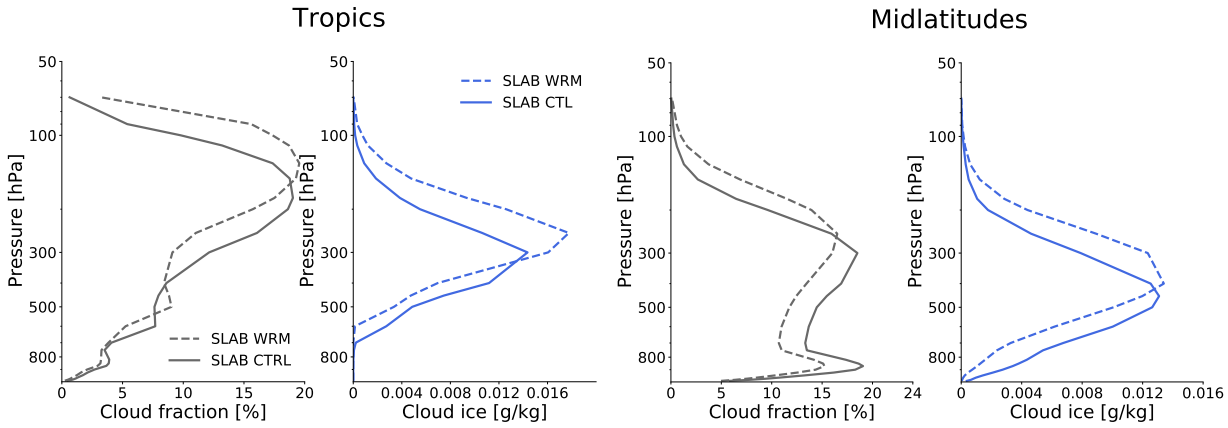

Figure 5.11: Vertical profile of cloud fraction and cloud ice against pressure in hPa for the SLAB simulation set under a quadrupling of CO_2 (WRM, dashed) and for the control simulation with 1xCO_2 (CTL, solid) for tropics (left) and midlatitudes (right). The values are averaged over 30°N-30°S for the tropics and over 30°-60°N and 30°-60°S for the midlatitudes.

5.3.2 Cloud-Radiative Heating Changes obtained from the PRP Calculations in SLAB

Now that we have closely analyzed the performance of the upward shift being able to capture future changes in cloud-radiative heating with the present-day cloud-radiative heating in ICON-ESM, calculated from the radiative flux divergences, we next want to compare this outcome to the cloud-radiative heating changes obtained with the partial-radiative perturbation calculations.

With the PRP calculations, it is possible to separate the cloud-radiative heating from the influences of the water vapor changes and clear sky temperature changes, which still play a role in the calculation of the cloud-radiative heating via the radiative flux divergences.

The radiative change arising from changes in water vapor (q) is depicted in the blue dashed line of Fig. 5.12 and shows the overall cooling effect in the upper troposphere and stratosphere for both the tropics and midlatitudes. The dashed purple line in Fig. 5.12 shows the combined effect of radiative chances in clouds and water vapor (qc), and therefore accounts for the nonlinear effects between these two.

Looking at Fig. 5.12 (left panel) for the tropics, we find that the qualitative pattern of the maximum at around 200 hPa and the minimum at 400 hPa is captured by the upward shift, but with an offset. The reason for the offset is probably the still strong increase in cloud ice in ICON-ESM depicted in Fig. 5.10. But because the overall values of cloud ice in our simulations are much higher than in Voigt et al. (2019), the increase of cloud ice under

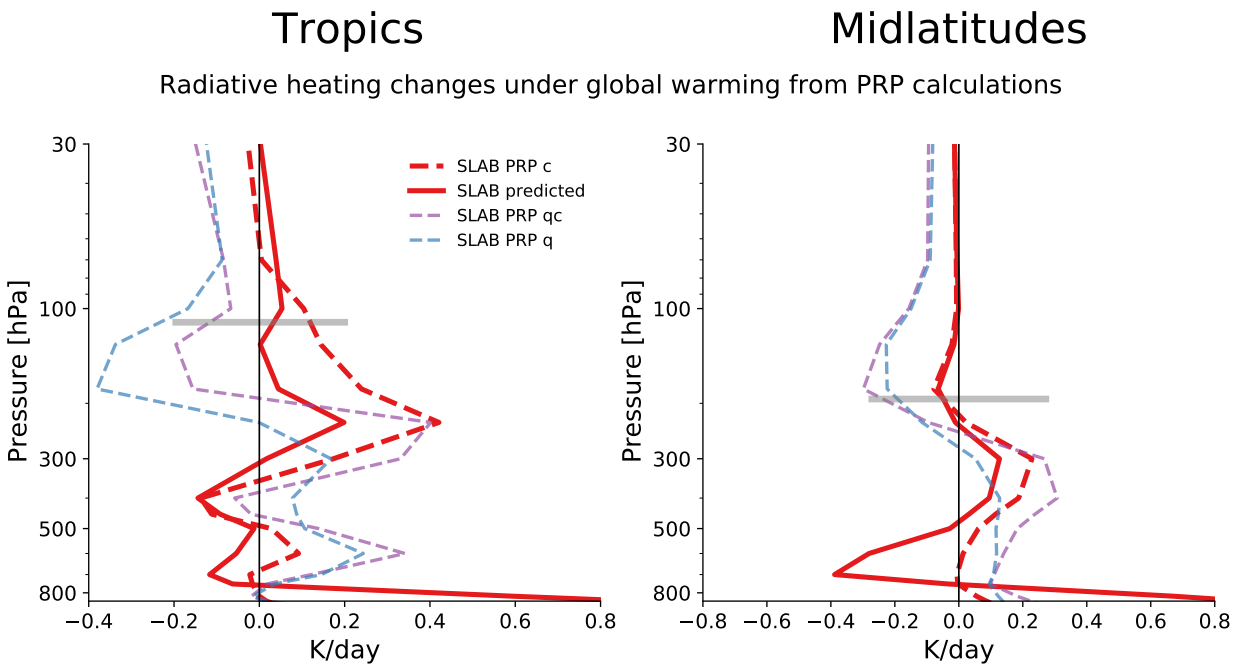

Figure 5.12: Radiative heating changes under a quadrupling of CO_2 from PRP calculations for the tropics (left) and the midlatutides (right) arising from clouds (c), water vapor (q) and the combined effect of both (qc). The solid red line is the same as in Fig. 5.9 and represents the changes in cloud radiative-heating under 4xCO_2, obtained through the upward shift of the present-day cloud-radiative heating. The gray horizontal bar depicts the level of the tropopause from CTL.

global warming is less significant in our simulations than in Voigt et al. (2019). The huge increase in cloud ice due to global warming was identified as the problem of ICON compared to the other models in Voigt et al. (2019). Because our results for ICON-ESM show a relative smaller increase in cloud ice under global warming, we find an improvement for the upward shift framework applied to the cloud-radiative heating changes from the PRP calculations compared to the ICON model, as used in Voigt et al. (2019).

For the midlatitudes in Fig. 5.12, compared to ICON, as used as in Voigt et al. (2019), the upward shift has less of an offset for the altitudes around the tropopause but more of an offset between 300 hPa and 500 hPa. Overall, this shows no improvement, but as mentioned before in the midlatitudes, it already worked well for all models in Voigt et al. (2019).

It is interesting to see that where the vertical profile of the present-day cloud ice in the tropics starts to increase strongly (Fig. 5.11 below 150 hPa) clouds start to dominate the shared impact depicted in the purple line, until it overlaps with the maximum of the cloud-radiative heating changes at 0.4 K^{-1}. Between 200 hPa and 400 hPa, qc is dominated by the changes in clouds above and below. Where cloud ice is low, the purple line follows the blue line, which depicts changes in water vapor. The same can be seen for the midlatitudes,

where clouds dominate the pattern of the purple line between 250 hPa and 500 hPa. This is in line with the areas of the maximum in zonal-mean atmospheric cloud-radiative heating in Fig. 5.3b. Overall, this shows the more or less linear relationship between clouds and qc on a global scale. Thus, we have confirmed that the PRP calculations can be meaningfully applied to separate the effect of ACRE as suggested in Bony et al. (2006).

Contrasting Fig. 5.9 with the results from the PRP calculations, we see that the cloud masking effect really is masking the cloud-radiative impact in terms of decreasing its magnitude. This is especially visible at the altitudes of the cloud ice maximum at 200 hPa for the tropics and 300 hPa for the midlatitudes. That means that cloud-radiative effects are an even stronger contributor to the circulation response when adjusted for the influence of water vapor and temperature in ICON-ESM.

To summarize our results for question 3, we find that:

1. ICON-ESM yields a more realistic vertical profile of the present-day cloud-radiative heating calculated from the all-sky minus clear-sky radiative fluxes, compared to the models analyzed in Voigt et al. (2019). Especially compared to ICON, as used in Voigt et al. (2019), the vertical profile of cloud-radiative heating has improved significantly for the tropics (Fig. 5.9). The reason for that is probably an improved parametrization of cloud ice and cloud water in the climate physics package compared to the physics package developed for numerical weather prediction, as used in Voigt et al. (2019).

2. The enhanced performance in representing cloud ice and cloud water may also lead to a better agreement between the cloud-radiative heating changes obtained from the upward shifted present-day cloud-radiative heating and the changes we find, contrasting global warming simulations with present-day simulations.

3. Regarding the isolated cloud impact with the PRP calculations, the upward shift manages to capture the qualitative pattern of the cloud-radiative heating changes, but shows an offset (Fig. 5.12). This offset does not occur in the analysis via the present-day and global warming radiative fluxes.

4. Interestingly, the upward shift still manages to capture the isolated cloud-radiative heating changes obtained from the PRP calculations, where dampening cloud masking effects are suppressed. Thus, our results suggest that the upward shift of the present-day cloud radiative heating is a robust feature in global warming simulations, compared with the analysis in Voigt et al. (2019).

6. Conclusion

Voigt et al. (2019) and Albern et al. (2019) have shown that clouds are an important contributor to climate change effects and its uncertainties regarding the representation and prediction in climate models, especially concerning changes in atmospheric circulation on a global as well as regional scale. Building upon their work, in this thesis, we conducted multiple simulations with an additional model setup, analyzing the cloud impact on the circulation change under global warming decomposed into the atmospheric and surface pathways. Our findings not only confirm the importance of changes in cloud radiation on the jet stream at a global scale, but also for the North Atlantic, the North Pacific and the Southern Hemisphere ocean basin. We now want to conclude and summarize our findings and specifically address the research questions once again.

Question 1

What is the role of clouds in setting the zonal-mean circulation response to warming on a global scale and how is the cloud impact distributed between the atmospheric and surface pathways?

On a global scale, our findings show that the atmospheric pathway of the cloud-radiative impact accounts for half of the total jet shift in both hemispheres. Because similar importance of the atmospheric pathway was found in Voigt et al. (2019), this highlights the importance of cloud-radiative changes in upper tropospheric ice clouds on the global circulation response under global warming across different models and experimental setups.

ICON-ESM depicts a more equal role for the atmospheric and surface pathways in setting the Northern Hemisphere jet shift than in Voigt et al. (2019). This can be related to a less pronounced dominance of the longwave radiation at the high northern latitudes in our simulations (Fig. 5.3c).

In our simulations, the surface pathway dominates the shift in the latitude of the subtropical dry zones in both hemispheres. ICON-ESM also shows less pronounced changes in the Hadley cell edges. Because the surface pathway is likely dominated by low-level clouds,

this may be a sign that midlatitude storm tracks in ICON-ESM have a greater influence on the shift of the subtropical dry zones than the drying effects of the strong subsidence from the Hadley cells.

Question 2

Focusing on the three ocean basins of the North Atlantic, North Pacific, and Southern Hemisphere, what is the relative role of the atmospheric and surface pathways in the jet response regionally?

Before we address Question 2, we will briefly discuss the reliability of the cloud-locking method. On a global scale it works well, showing small residuals. On a regional scale, however, the residuals for the North Pacific and North Atlantic are significant, which can be seen in Fig. 5.6, Fig. 5.7, Fig. 5.8 and in the Appendix. Especially for the North Atlantic, the total free jet response is just approximately half of the total locked jet shift in all three simulation sets SLAB, SSTSLAB and SSTCLIM.

In Albern et al. (2019) it has been found that for the North Pacific and the SH, the internal model variability is small. They showed that the difference in the jet shift for the free and locked simulations in the annual mean are close to 0 and statistically similar in most seasons at a 95% significance level. But for the North Atlantic, the internal model variability was high, and the difference in the jet shift between the free and locked simulations in the annual-mean was around -2°. Most of these inconsistencies have been found to arise from the spring season from March to May (MAM), depicting differences in the jet latitude of -7.5° in the statistical mean based on a bootstrap distribution (text S1 and figure S3 of Albern et al. (2019)). Our results show that big residuals in this region remain, even if we couple ICON-ESM to a slab ocean and use the climate physics package.

Although the residuals increase on a regional level, the cloud impact dominates the total jet shift in the SLAB and SSTCLIM simulation sets, contributing half of the total jet shift when the surface pathway is switched off in SSTSLAB. Moreover, the cloud impact shows the same sign across all simulation pairs for the jet shift and the jet strengthening, except for the jet strengthening in the North Pacific in SLAB and SSTCLIM, which can be seen in the Appendix. This signals a high degree of certainty about the sign of the cloud impact on the atmospheric circulation change at global and regional scales as well as for the atmospheric pathway and surface pathway.

The cloud-radiative impact also contributes most to the zonally symmetric jet response, showing a zonally symmetric pattern around the jet latitude across all simulations for the

combined activity of the surface and atmospheric pathways but also for the atmospheric pathway isolated. Changes in water vapor and SST/CO_2 do not show a zonally symmetric impact on the jet latitude to the same extent. This points out that the cloud impact is especially relevant in climate models for assessing the magnitude of future changes in the global and regional jet latitudes. Similar importance of the cloud impact on the circulation change under a doubling of CO_2 was also found for two CMIP5 models coupled to a slab ocean in Ceppi and Shepherd (2017).

Regarding the jet strengthening under a quadrupling of CO_2, clouds account for roughly two thirds of the total strengthening from the locked simulations of ≈ 1.2 m s^{-1} in the North Atlantic and of ≈ 1.8 m s^{-1} the Southern Hemisphere. The total locked jet strengthening of ≈ 0.2 m s^{-1} in the North Pacific is found to be much smaller. The isolated atmospheric pathway in SSTSLAB still accounts for roughly half of the total locked jet strengthening for the SH and for one third in the North Atlantic. In Albern et al. (2019), the jet strengthening for the North Pacific was also found to be much smaller then for the North Atlantic and SH. Whereas the atmospheric pathway for a uniform 4-K SST increase also accounted for approximately half of the total locked jet strengthening in Albern et al. (2019).

Question 3

What are the changes in cloud-radiative heating in ICON-ESM under global warming, and are these changes captured by an upward shift of the present-day cloud-radiative heating?

Whereas the models in Voigt et al. (2019) showed huge discrepancies, our results are in better agreement with the vertical profile of the present-day cloud-radiative heating, obtained from measurements with *CloudSat/CALIPSO* (Fig. 5.9). This is a promising improvement to the ICON setup used in Voigt et al. (2019) and most likely is due to an enhancement in the representation of cloud ice.

We tested if that improvement also leads to a higher agreement between the upward shifted present-day cloud-radiative heating changes and the changes obtained by contrasting the present-day and future cloud-radiative heating profiles. We derived the cloud-radiative heating changes from the all-sky minus clear-sky fluxes, as well as from the PRP calculations. For the PRP calculations compared to ICON, as used in Voigt et al. (2019), ICON-ESM version 2.6.2.2 with the climate physics package is now able to capture the qualitative pattern of the cloud-radiative heating changes with the upward shift framework, although with an offset (Fig. 5.12). This offset points to the cloud masking effects of water vapor and temperature, which are still present in the upward-shifted present-day cloud-radiative heating changes.

Our findings confirm that differences in representing the upper-tropospheric cloud-radiative heating in present-day simulations across models can translate to differences in changes in upper-tropospheric cloud-radiative heating under global warming as proposed in Voigt et al. (2019). With our study, we emphasize the robust and significant impact of rising high level clouds on the atmospheric circulation change in climate models.

In Voigt et al. (2019) a clear link between differences in the magnitude of the atmospheric pathway and differences in cloud-radiative heating changes has been found and is supported by our results with the upward shift in ICON-ESM. Therefore, we confirm the suggestion of Voigt et al. (2019) that a constraint of the atmospheric pathway through observations and global climate models could help to decrease intermodel spread in atmospheric circulation changes. This could help improve model predictions of regional climate change.

7. Outlook

Many studies have shown that the atmospheric CRE of rising high-level clouds is likely a new robust thermodynamic constraint on climate change diagnostics (e.g. Li et al., 2019; Albern et al., 2019; Voigt et al., 2019). We want to emphasize the proposal of Voigt et al. (2021) that incorporating diagnostics for the vertical structure of the atmospheric cloud-radiative heating into intercomparison studies would allow for a more comprehensive analysis of the radiative coupling between clouds and the atmospheric circulation. A wide variety of data about the vertical structure of the atmospheric cloud-radiative heating available from different models could be important for constraining model biases and intermodel spread.

It was found that the cloud impact is responsible for much of the annual-mean zonal-mean wind change under global warming in Voigt et al. (2019) as well as in our simulations. But not just the jet shift is relevant for being able to account for the effects of global warming on a regional scale, but also its variability. It would be interesting to evaluate how the cloud impact changes the pattern of the meandering jet stream, not just for the jet latitude and speed, but also for the zonal extent of the Rossby waves. This could, for example, be accomplished by applying the EOF method used in Barnes and Polvani (2013) on the jet response of the atmospheric and surface pathways in our results for ICON-ESM. In this way, it might be possible to gain further insight into how low and high-level clouds impact internal jet variability.

The cloud-locking method applied to the model version 2.6.2.2 of ICON, even coupled to a slab ocean, still yields large residuals in the North Atlantic. Therefore, it would possibly be revealing to repeat the bootstrap distributions analysis on a seasonal basis as conducted in Albern et al. (2019). This way, intermodel variability and decorrelation effects regarding the cloud-locking method could be attributed to specific seasons and regions. Thus, changes in the atmospheric circulation and how they are affected by the atmospheric and surface pathways, specifically the magnitude of the jet response, would be more reliable and easier to interpret.

A further investigation of the atmospheric and surface pathways concerning seasonal changes would be interesting in general, because fewer studies have been conducted on a seasonal

basis and none for the decomposed effects of the surface and atmospheric pathways. However, these are needed to assess the impact of regional changes in atmospheric circulation and their physical dependencies.

A. Appendix

In the Appendix, we document the individual estimates of the cloud, water vapor, and SST/CO_2 impact from the cloud-locking method in our simulations. In the main part of the thesis, we use the averaged values.

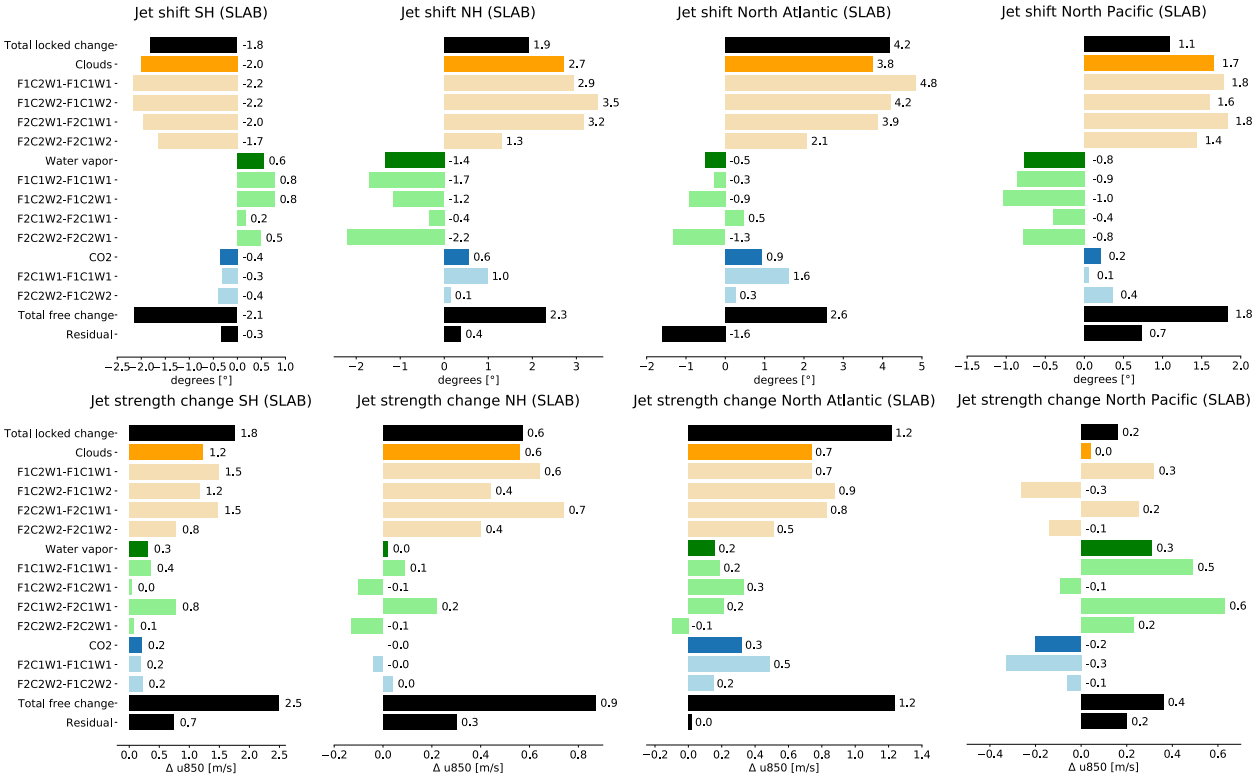

Figure A.1: Changes in jet latitude and jet strength for total free and total locked response (black bars) in the SLAB simulation set, as well as the response for all simulation pairs decomposed into the cloud impact (orange), the water vapor impact (green) and the CO_2 impact (blue), depicted for the SH, NH, North Atlantic, and North Pacific. The values of the responses are printed on the right hand side of each bar.

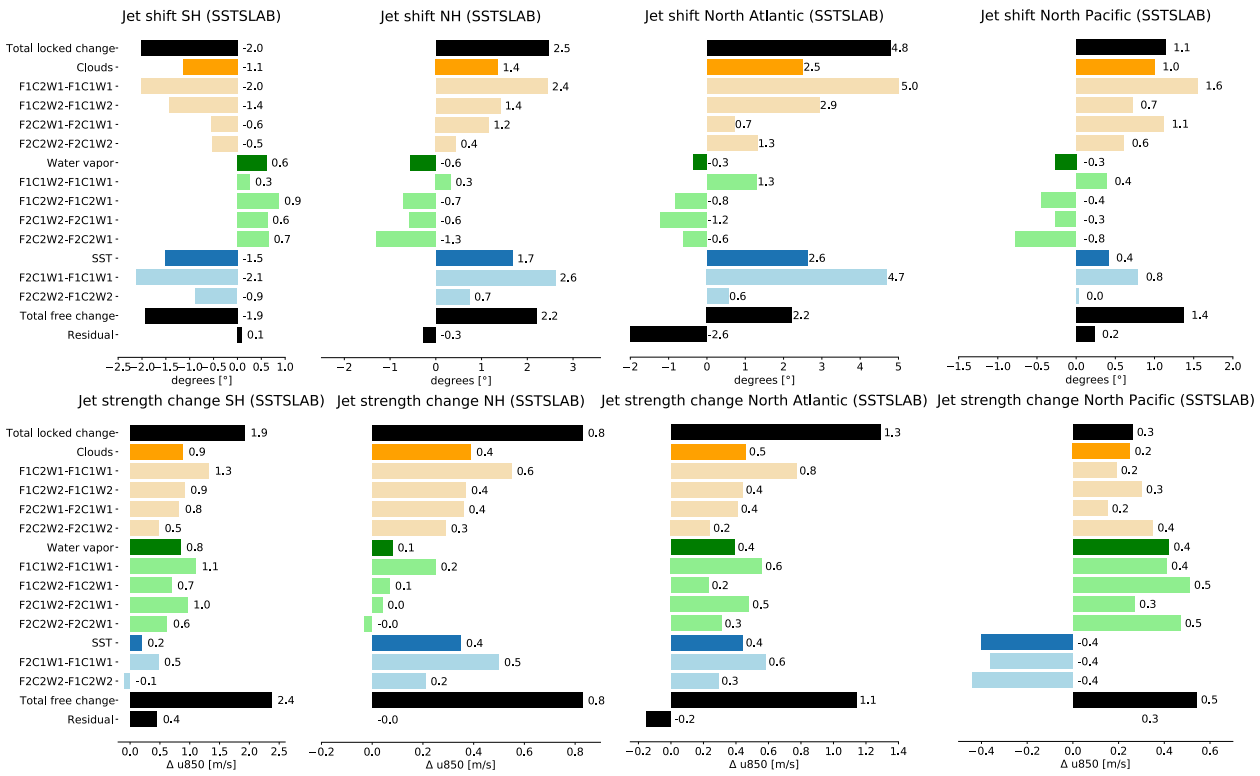

Figure A.2: Changes in jet latitude and jet strength for total free and total locked response (black bars) in the SSTSLAB simulation set, as well as the response for all simulation pairs decomposed into the cloud impact (orange), the water vapor impact (green) and the SST impact (blue), depicted for the SH, NH, North Atlantic, and North Pacific. The values of the responses are printed on the right hand side of each bar.

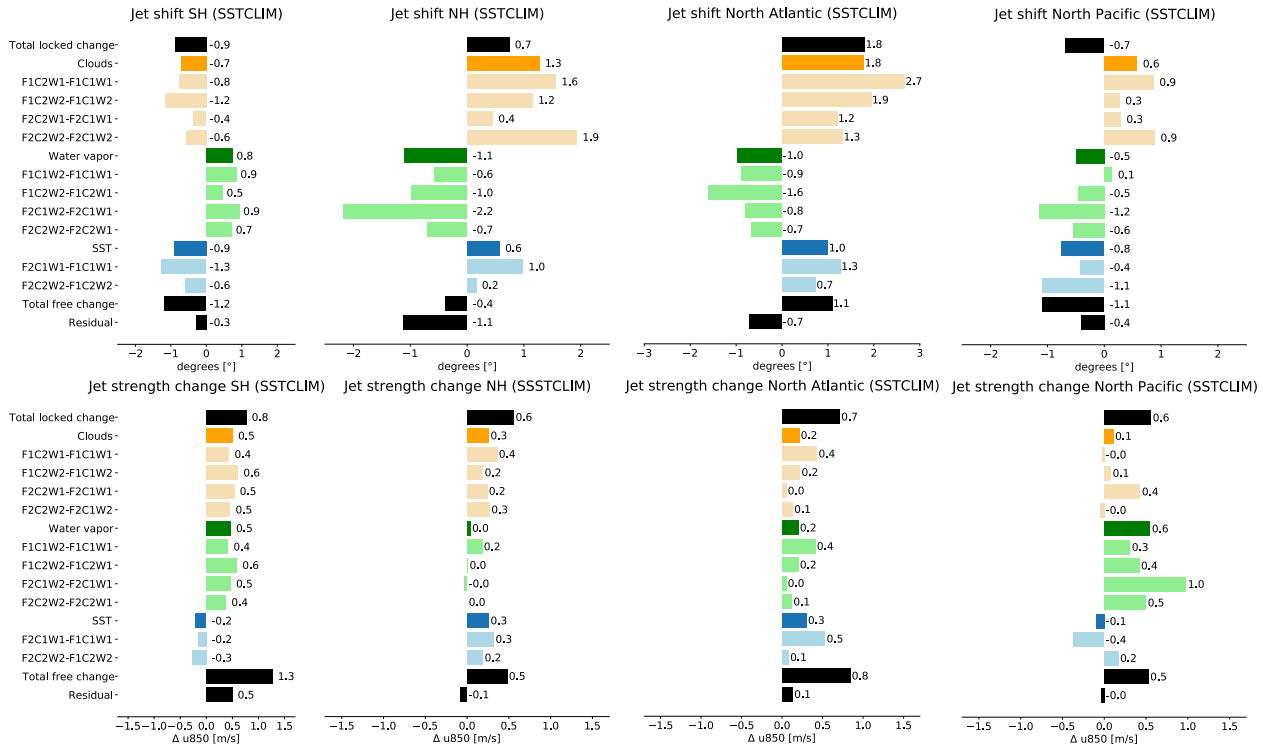

Figure A.3: Changes in jet latitude and jet strength for total free and total locked response (black bars) in the SSTCLIM simulation set, as well as the response for all simulation pairs decomposed into the cloud impact (orange), the water vapor impact (green) and the SST impact (blue), depicted for the SH, NH, North Atlantic, and North Pacific. The values of the responses are printed on the right hand side of each bar.

B. List of Figures

Bibliography

Albern, N., Voigt, A., and Pinto, J. G. (2019). Cloud-radiative impact on the regional responses of the midlatitude jet streams and storm tracks to global warming. *Journal of Advances in Modeling Earth Systems, 11,1940–1958.*

Albern, N., Voigt, A., Thompson, D. W. J., and Pinto, J. G. (2020). The role of tropical, midlatitude, and polar cloud-radiative changes for the midlatitude circulation response to global warming. *Journal of Climate*, 33(18):7927–7943.

Barnes, E. A. and Polvani, L. (2013). Response of the midlatitude jets, and of their variability, to increased greenhouse gases in the CMIP5 models. *Journal of Climate*, 26(18):7117–7135.

Bony, S., Colman, R., Kattsov, V. M., Allan, R. P., Bretherton, C. S., Dufresne, J.-L., Hall, A., Hallegatte, S., Holland, M. M., Ingram, W., Randall, D. A., Soden, B. J., Tselioudis, G., and Webb, M. J. (2006). How well do we understand and evaluate climate change feedback processes? *Journal of Climate*, 19(15):3445–3482.

Brient, F., Roehrig, R., and Voldoire, A. (2019). Evaluating marine stratocumulus clouds in the CNRM-CM6-1 model using short-term hindcasts. *Journal of Advances in Modeling Earth Systems*, 11(1):127–148.

Butler, A. H., Thompson, D. W. J., and Heikes, R. (2010). The steady-state atmospheric circulation response to climate change–like thermal forcings in a simple general circulation model. *Journal of Climate*, 23(13):3474–3496.

Ceppi, P. and Shepherd, T. G. (2017). Contributions of climate feedbacks to changes in atmospheric circulation. *Journal of Climate*, 30(22):9097–9118.

Ceppi, P., Zelinka, M. D., and Hartmann, D. L. (2014). The response of the Southern Hemispheric eddy-driven jet to future changes in shortwave radiation in CMIP5. *Geophysical Research Letters*, 41(9):3244–3250.

Chang, E. K. M., Lee, S., and Swanson, K. L. (2002). Storm track dynamics. *Journal of Climate*, 15(16):2163–2183.

Colman, R. A., Power, S. B., and McAvaney, B. J. (1997). Non-linear climate feedback analysis in an atmospheric general circulation model. *Climate Dynamics*, 13(10):717–731.

Eyring, V., Bony, S., Meehl, G. A., Senior, C. A., Stevens, B., Stouffer, R. J., and Taylor, K. E. (2016). Overview of the Coupled Model Intercomparison Project phase 6 (CMIP6) experimental design and organization. *Geoscientific Model Development*, 9(5):1937–1958.

Fu, Q. and Liou, K. N. (1993). Parameterization of the radiative properties of cirrus clouds. *Journal of Atmospheric Sciences*, 50(13):2008–2025.

Gates, W. L. (1992). An ams continuing series: Global change–amip: The Atmospheric Model Intercomparison Project. *Bulletin of the American Meteorological Society*, 73(12):1962–1970.

Grise, K. M. and Medeiros, B. (2016). Understanding the varied influence of midlatitude jet position on clouds and cloud radiative effects in observations and global climate models. *Journal of Climate*, 29(24):9005–9025.

Grise, K. M. and Polvani, L. M. (2014). The response of midlatitude jets to increased CO2: distinguishing the roles of sea surface temperature and direct radiative forcing. *Geophysical Research Letters*, 41(19):6863–6871.

Grise, K. M. and Polvani, L. M. (2016). Is climate sensitivity related to dynamical sensitivity? *Journal of Geophysical Research: Atmospheres*, 121(10):5159–5176.

Hartmann, D. L. (2007). The atmospheric general circulation and its variability. *Journal of the Meteorological Society of Japan. Ser. II*, 85B:123–143.

Hartmann, D. L. and Larson, K. (2002). An important constraint on tropical cloud - climate feedback. *Geophysical Research Letters*, 29(20):12–1–12–4.

Held, I. M. and Hou, A. Y. (1980). Nonlinear axially symmetric circulations in a nearly inviscid atmosphere. *Cover Journal of the Atmospheric Sciences 37(3)*, pages 515–533.

Hoskins, B. J. and Valdes, P. J. (1990). On the existence of storm-tracks. *Journal of Atmospheric Sciences*, 47(15):1854–1864.

Kinne, S., O'Donnel, D., Stier, P., Kloster, S., Zhang, K., Schmidt, H., Rast, S., Giorgetta, M., Eck, T. F., and Stevens, B. (2013). MAC-v1: a new global aerosol climatology for climate studies. *Journal of Advances in Modeling Earth Systems*, 5(4):704–740.

Kornhuber, K. and Tamarin-Brodsky, T. (2021). Future changes in northern hemisphere summer weather persistence linked to projected arctic warming. *Geophysical Research Letters*, 48(4):e2020GL091603. e2020GL091603 2020GL091603.

Lang, J.-P. (2021). ICON: Icosahedral nonhydrostatic weather and climate model. Url: https://code.mpimet.mpg.de/projects/iconpublic. Last call: 21.12.2021.

Lehner, F., Deser, C., Maher, N., Marotzke, J., Fischer, E. M., Brunner, L., Knutti, R., and Hawkins, E. (2020). Partitioning climate projection uncertainty with multiple large ensembles and CMIP5/6. *Earth System Dynamics*, 11(2):491–508.

Li, Y., Thompson, D. W. J., Bony, S., and Merlis, T. M. (2019). Thermodynamic control on the poleward shift of the extratropical jet in climate change simulations: The role of rising high clouds and their radiative effects. *Journal of Climate*, 32(3):917–934.

Mauritsen, T., Stevens, B., Roeckner, E., Crueger, T., Esch, M., Giorgetta, M., Haak, H., Jungclaus, J., Klocke, D., Matei, D., Mikolajewicz, U., Notz, D., Pincus, R., Schmidt, H., and Tomassini, L. (2012). Tuning the climate of a global model. *Journal of Advances in Modeling Earth Systems*, 4(3):M00A01.

Max-Planck-Gesellschaft (MPG) zur Förderung der Wissenschaften e.V. (2017). ICON-ESM – das MPI-M-Erdsystemmodell der nächsten generation. Url: https://mpimet.mpg.de/kommunikation/im-fokus/icon-erdsystemmodell. Last call: 21.12.2021.

Miao, H., Wang, X., Liu, Y., and Wu, G. (2021). A regime-based investigation into the errors of CMIP6 simulated cloud radiative effects using satellite observations. *Geophysical Research Letters*, 48(18):e2021GL095399.

National Aeronautics and Space Administration (2022). The afternoon constellation. Url: https://atrain.nasa.gov/. Last call: 31.03.2022.

Pfleiderer, P., Schleussner, C.-F., Kornhuber, K., and Coumou, D. (2019). Summer weather becomes more persistent in a 2°C world. *Nature Climate Change*, 9(9):666–671.

Philip, S. Y., Kew, S. F., van Oldenborgh, G. J., Anslow, F. S., Seneviratne, S. I., Vautard, R., Coumou, D., Ebi, K. L., Arrighi, J., Singh, R., van Aalst, M., Marghidan, C. P., Wehner, M., Yang, W., Li, S., Schumacher, D. L., Hauser, M., Bonnet, R., Luu, L. N., Lehner, F., Gillett, N., Tradowsky, J., Vecchi, G. A., Rodell, C., Stull, R. B., Howard, R., and Otto, F. E. L. (2021). Rapid attribution analysis of the extraordinary heatwave on the pacific coast of the US and Canada June 2021. *Earth Syst. Dynam. Discuss. [preprint], in review*, 2021:1–34. Url: https://doi.org/10.5194/esd-2021-90.

Rubel, F., Brugger, K., Haslinger, K., and Auer, I. (2017). The climate of the European Alps: Shift of very high resolution Köppen-Geiger climate zones 1800–2100. *Meteorologische Zeitschrift*, 26(2):115–125.

Rubel, F. and Kottek, M. (2010). Observed and projected climate shifts 1901-2100 depicted by world maps of the köppen-geiger climate classification. *Meteorologische Zeitschrift*, 19:135–141.

Shaw, T. A. (2019). Mechanisms of future predicted changes in the zonal mean mid-latitude circulation. *Current Climate Change Reports*, 5(4):345–357.

Shaw, T. A., Baldwin, M., Barnes, E. A., Caballero, R., Garfinkel, C. I., Hwang, Y.-T., Li, C., O'Gorman, P. A., Rivière, G., Simpson, I. R., and Voigt, A. (2016). Storm track processes and the opposing influences of climate change. *Nature Geoscience*, 9:656–664.

Siebesma, A. P., Bony, S., Jakob, C., and Stevens, B., editors (2020). *Clouds and Climate Climate Science's: Greatest Challenge*. Cambridge University Press.

Singh, M. S. and O'Gorman, P. A. (2012). Upward shift of the atmospheric general circulation under global warming: Theory and simulations. *Journal of Climate*, 25(23):8259–8276.

Soden, B. J., Broccoli, A. J., and Hemler, R. S. (2004). On the use of cloud forcing to estimate cloud feedback. *Journal of Climate*, 17(19):3661 – 3665.

Taylor, K. E., Stouffer, R. J., and Meehl, G. A. (2012). An overview of CMIP5 and the experiment design. *Bulletin of the American Meteorological Society*, 93(4):485–498.

Thompson, D. W. J., Bony, S., and Li, Y. (2017). Thermodynamic constraint on the depth of the global tropospheric circulation. *Proceedings of the National Academy of Sciences*, 114(31):8181–8186.

Tompkins, A. M. (2005). The parametrization of cloud cover. *ECMWF Moist Processes Lecture Note Series, ECMWF Technical Memoranda*.

Voigt, A., Albern, N., Ceppi, P., Grise, K., Li, Y., and Medeiros, B. (2021). Clouds, radiation, and atmospheric circulation in the present-day climate and under climate change. *WIREs Climate Change*, 12(2):e694.

Voigt, A., Albern, N., and Papavasileiou, G. (2019). The atmospheric pathway of the cloud-radiative impact on the circulation response to global warming: Important and uncertain. *Journal of Climate, 32(10)*, page 3051–3067.

Voigt, A. and Shaw, T. A. (2016). Impact of regional atmospheric cloud radiative changes on shifts of the extratropical jet stream in response to global warming. *Journal of Climate*, 29(23):8399–8421.

Wetherald, R. T. and Manabe, S. (1988). Cloud feedback processes in a general circulation model. *Journal of Atmospheric Sciences*, 45(8):1397–1416.

Yin, J. H. (2005). A consistent poleward shift of the storm tracks in simulations of 21st century climate. *Geophysical Research Letters*, 32(18):L18701.

Zelinka, M. D., Myers, T. A., McCoy, D. T., Po-Chedley, S., Caldwell, P. M., Ceppi, P., Klein, S. A., and Taylor, K. E. (2020). Causes of higher climate sensitivity in CMIP6 models. *Geophysical Research Letters*, 47(1):e2019GL085782.

Acknowledgments

I want to say thank you to my supervisors, Aiko Voigt and Nicole Albern, who accompanied me on my way last year and were a great support. They always had an open ear for my questions, and without their help, professionalism, and insight, I could not have done this Masters Thesis. I am especially grateful to my co-supervisor, Nicole Albern, for her continuous assistance, even though she changed positions during the process. Thank you for supporting me all the way. I would also like to say thank you to all the other team members of Aiko Voigt's research group. I'm really glad I was able to meet them and get to know them. The group meetings enabled fruitful discussions and offered the possibility to ask questions. Above all, they also offered an opportunity for interpersonal exchange, which has taken on even greater significance than usual in the last few Corona years and for which I am very grateful. Finally, I want to say thank you to my girlfriend, Melanie, my family, and my friends. Thank you for being there for me in challenging times and always believing in me.